A Corrosion Monitoring System for Existing Reinforced Concrete Structure
Final Report

Prepared By:
Xianming Shi
Zhirui Ye
Anburaj Muthumani
Yida Fang
Yan Zhang
Western Transportation Institute
Montana State University
Hui Yu
Southwest Rsearch Institute

June 30, 2013

REPORT DOCUMENTATION PAGE	Form approved OMB No.

Public reporting for this collection of information is estimated to average 1 hour per response, including the time for reviewing instructions, searching existing data sources, gathering and maintaining the data needed, and completing and reviewing the collection of information. Send comments regarding this burden estimate or any other aspect of this collection of information, including suggestion for reducing this burden to Washington Headquarters Services, Directorate for Information Operations and Reports, 1215 Jefferson Davis Highway, Suite 1204, Arlington, VA 22202-4302, and to the Office of Management and Budget, Paperwork Reduction Project (0704-1833), Washington, DC 20503

1. AGENCY USE ONLY (LEAVE BLANK)	2. REPORT DATE December 2012	3. REPORT TYPE AND DATES COVERED Final Report (08/18/2011-12/31/2012)	

4. TITLE AND SUBTITLE A Corrosion Monitoring System for Existing Reinforced Concrete Structures	5. FUNDING NUMBERS AUTC# 510000 DTRT06-G-0011
6. AUTHOR(S) Xianming Shi, Zhirui Ye, Anburaj Muthumani, Yida Fang, Yan Zhang	

7. PERFORMING ORGANIZATION NAME(S) AND ADDRESS(ES) Alaska University Transportation Center P.O. Box 755900 Fairbanks, AK 99775-5900	8. PERFORMING ORGANIZATION REPORT NUMBER INE/AUTC 12.36
Research and Innovative Technology Administration (RITA) U.S. Dept. of Transportation (USDOT) 1200 New Jersey Ave, SE, Washington DC, 20590 Oregon Department of Transportation: Research Section 555 13th Street NE, Suite 2, Salem, OR 97301-5192	10. SPONSORING/MONITORING AGENCY REPORT NUMBER

11. SUPPLENMENTARY NOTES

12a. DISTRIBUTION / AVAILABILITY STATEMENT No restrictions	12b. DISTRIBUTION CODE

13. ABSTRACT (Maximum 200 words)

Reinforced concrete is utilized in a wide spectrum of transportation infrastructure but may suffer significantly from unrecognized corrosion in cold weather regions. Addressing AUTC's mission of maintaining cold region transportation systems, AUTC Director Billy Connor is working with Dr. Xianming Shi, PhD, P.E., director of the TWI Corrosion and Sustainable Infrastructure Lab at Montana State University-Bozeman, on research to develop a reliable, cost-effective corrosion monitoring system from existing reinforced concrete (RC) transportation structures. The technology resulting from the project will provide a lower cost system for existing Department of Transportation RC structures in aggressive service environments, offering higher quality carion condition information. T will also detect corrosion initiation and propagation in the RC structures at the earliest possible time, enabling condition-based maintenance strategies.

Connor and Shi hope to reach four specific objectives in their research of RC structures: 1) improve and validate the SwRI corrosion sensor prototype for concrete corrosion monitoring systems; 2) develop algorithms for quality control and sensor data interpretation; 3) make viable implementation recommendations for corrosion monitoring systems and existing DOT inventory of RC bridges; and 4) deliver a deployable prototype corrosion sensing system for DOTs to continue field evaluations.

14- KEYWORDS: Corrosion protection (Fccmc), Corrosion resistant materials (Rbmdyse), Structural health monitoring (Grs), Corrosion (Scph), Monitoring (Dmbm)	15. NUMBER OF PAGES 69
	16. PRICE CODE N/A

17. SECURITY CLASSIFICATION OF REPORT Unclassified	18. SECURITY CLASSIFICATION OF THIS PAGE Unclassified	19. SECURITY CLASSIFICATION OF ABSTRACT Unclassified	20. LIMITATION OF ABSTRACT N/A

NSN 7540-01-280-5500

STANDARD FORM 298 (Rev. 2-98)
Prescribed by ANSI Std. 239-18 298-1

Table of Contents

List of Figures

List of Tables

Acknowledgements

Abstract

This study has developed and evaluated in the laboratory a multi-parameter corrosion monitoring system for existing reinforced concrete structures in chloride-laden service environments. The study improved and validated the SwRI corrosion sensor prototype for use in the concrete corrosion monitoring system; developed algorithms for quality control and interpretation of the sensor data; made viable recommendations to implement the corrosion monitoring system for existing DOT inventories of RC bridges; and delivered a deployable prototype corrosion sensing system for DOTs to continue field evaluations. The performance and reliability of the SwRI corrosion sensor were confirmed by the benchmark test in simulated concrete pore solutions. However, once active corrosion is initiated and a great amount of chloride is present, the multi-electrode array sensor (MAS) probe may no longer serve as a good tool to predict the corrosion rate of rebar unless more research is conducted to establish such prediction or correlation. The performance and reliability of the SwRI corrosion sensor were also confirmed by embedding it in a paste specimen, while some issues with firmware and possibly graphite reference probe were identified. While more research is needed, the paste specimen test also imply that the MAS probes, Cl probes and pH probes all have great potential to work properly under a reasonably low electric field.

At the WTI CSIL, the custom-made chloride probes along with the SwRI sensor, a conventional Ag/AgCl probe (as control), and three rust-free, bare steel #4 rebars went through a cyclic immersion in the simulated concrete pore solutions. For the 9-pin MAS, the following three parameters showed strong correlation with the chloride concentration of the simulated pore solutions: (1) *maximum of maximum ΔE*, (2) *maximum of average ΔE*, and (3) *average of average ΔE / average of maximum ΔE*. For the 6-pin MAS, the following three parameters showed strong correlation with the chloride concentration of the simulated pore solutions: (1) *average of maximum ΔE*, (2) *average of average ΔE*, and (3) *average of average ΔE / maximum of maximum ΔE*. The 3rd parameter may hold the promise of using 6-pin MAS as a very good tool to predict the rebar corrosion rate even in the case of active corrosion and high chloride concentration, which warrant additional research. Only one of the three SwRI Ag/AgCl probes was found to be reliable chloride probes after the eight cycles of weathering. This highlight the need for further improving the approach to fabricate the Ag/AgCl probes to serve as chloride probes in concrete. Meanwhile, three WTI custom-made chloride probes (with the appropriate treatment by proprietary coating) showed great promise in this regard. Only one of the three SwRI graphite probes remained relatively stable over the eight cycles of weathering, with its potential showing a standard deviation of 11 mV and a COV of -6%. Interestingly, a few of the WTI custom-made Ag/AgCl probes showed good potential to serve as reliable reference electrodes in concrete. The vast majority of the sensing probes featured a response time of less than 60 seconds.

Suggested Research

- Additional optional phases of this project should focus on improving the system reliability, usability and cost-effectiveness.

- Additional research should examine the feasibility to use a certain parameter from the 6-pin MAS probes, such as *average of average ΔE / maximum of maximum ΔE* or certain

index calculated from the MAS probe readings (e.g., localized index using the software of *electrochemical noise analysis*) to reliably predict the rebar corrosion rate even in the case of active corrosion and high chloride concentration.

- Research is warranted to evaluate the combined use of the developed corrosion sensing system with ICCP to automatically adjust the protective current in a way that maximizes anode life and optimizes corrosion control. This may also entail the strategic placement of the sensing probes.

CHAPTER 1 – INTRODUCTION AND RESEARCH APPROACH

1.1. Problem Statement

Reinforcement corrosion induced by chloride contamination is a leading cause of structural damage and premature degradation in reinforced concrete (RC) structures. Approximately 90,000 bridges built in the United States are classified structurally deficient and/or functionally obsolete, representing approximately 15% of the total number of bridges in the country. Remediation projects for concrete bridges undertaken as a direct result of chloride-induced rebar corrosion was estimated to cost U.S. highway departments $5 billion per year, aside from the safety and reliability implications. Concern is the greatest in coastal and northern states where these structures are exposed to marine environments and deicing salts, respectively, such as in the state of Oregon. ODOT has historic RC bridges along the Pacific coast that experience serious corrosion and degradation. Like other DOTs, ODOT is faced with the difficult and expensive task of more frequent routine corrosion inspection of aging infrastructure to enhance on-time maintenance decision making. Alaska DOT&PF also has corrosion concerns for structures in marine environments and older structures with cast-in-place concrete decks subject to deicing salts.

Currently, ODOT conducts labor-intensive corrosion surveys of its coastal bridges to determine the timing and type of remedial action they require. For instance, Figure 1 shows a typical corrosion damage pattern for ODOT coastal bridges. Consequently, ODOT tends to focus on obtaining chloride content profiles and rebar corrosion status on the side of the girder near the bottom where corrosion damage is most likely. This would be a likely location to embed corrosion sensors. A method of obtaining frequent corrosion information would provide better condition assessment at much lower cost than the periodic hands-on surveys. In addition, a system that monitors real-time corrosion behavior could be used in conjunction with impressed current cathodic protection (ICCP) to automatically adjust the protective current in a way that maximizes anode life and optimizes corrosion control.

Figure 1. Two photos of the same reinforced concrete girder showing no concrete damage on the ocean-facing side (left) and corrosion damage on the face of the beam opposite the ocean (right).

1.2. Problem Background

The inherent drawbacks of current corrosion sensors are their inability to effectively monitor the overall evolution of corrosion in RC structures and to detect or quantify the corrosion risk prior to corrosion initiation. Currently available commercial or laboratory prototype sensors

for rebar corrosion are typically placed in new structures during casting and, thus, are not suitable for corrosion sensing of existing RC structures. Arguably, corrosion sensors are most needed for existing structures that have endured decades of environmental exposure conditions (e.g., high humidity/wetness and chloride contents) and are faced with an *imminent* risk of rebar corrosion and concrete cracking. All currently available sensors have their limitations. For example, some are too large to be embedded in existing structures or they have an insufficient number of sensor types to illustrate the full picture of the rebar–concrete interfacial environment and associated corrosion risk. The longevity and reliability of these sensors are questionable inside concrete over extended periods within aggressive environments. Furthermore, corrosion damage inside concrete is difficult to detect particularly at the initiation stage. The use of real-time data for corrosion diagnosis and prognosis is still relatively unexplored and the ability to intelligently interrogate the multi-parameter, time-series, noise-containing sensor data is currently lacking. Embeddable sensors for on-line monitoring of multiple concrete state variables presents a great opportunity for the structural health monitoring of RC structures considering the abundance of data available for mining. A significant challenge for infrastructure managers and maintenance personnel is the ability to analyze sensor data and make informed maintenance decisions. Finally, interrogation of sensor systems requiring manual connection or wireless communication with limited range makes it difficult to collect sensor data, which is especially true in hidden or hard-to-inspect locations.

In light of the aging infrastructure and dwindling maintenance budgets, it is necessary to develop a small, reliable, embedded, multi-parameter sensor system to be deployed at distributed locations of existing RC structures that can capture the critical data indicative of chloride ingress, corrosion initiation and possibly early-age corrosion propagation. Such an effective, adaptive, field-deployable system can meet the urgent ODOT needs for corrosion monitoring, detection, and diagnosis as well as for the assessment of the remaining life of RC structures.

Working Technology for the Proposed Sensing System

This section will briefly describe the working technology underlying each of the sensing elements in the proposed sensing system. For the sensor prototype, the sensing elements will include a 9-pin Multielectrode Array Sensor (MAS) probe at rebar depth and chloride probes at various depths in concrete along with a reference probe. Sensing elements for other parameters, such as corrosion potential (E_{corr}), temperature, moisture, and pH, may be incorporated in an advanced version, if needed. According to the discussions with the project technical advisory committee (TAC), concrete carbonation is not a big concern in Oregon. The pH of solutions in concrete generally does not fluctuate significantly and thus could be measured periodically. Furthermore, in our lab and field studies, we will measure the pH and temperature inside the concrete at the same depth, with probes separate from the integrated corrosion sensing system. Data from such measurements will be fed into the final data analysis. While MAS or a separate sensing element could be used to monitor the E_{corr} of simulated rebar in concrete, the sensing of E_{corr} is less important than that of the corrosion rate of the simulated rebar and the chloride content depth profile in concrete. Similarly, while the moisture content in concrete is a key parameter to the corrosion risk, it is reflected in the corrosion rate data.

A graphite rod will be used as the pseudo-reference electrode in concrete as its electrochemical potential is relatively insensitive to the local contents of chloride and hydroxyl ions. A custom-made silver/silver chloride (Ag/AgCl) electrode will be used as the chloride probe in concrete. A Ag/AgCl electrode is used as a non-destructive tool in analytical chemistry to quantitatively determine the free chloride concentration or to continuously monitor its temporal evolution in aqueous solutions. The electrochemical potential of the chloride probe, measured against a stable reference electrode in the same environment, shows a strong linear relationship with the logarithm of the chloride activity (a_{Cl^-}). This relationship is known to follow the Nernst equation. The a_{Cl^-} can be reasonably approximated as chloride concentration when the sensor is placed in concentrations with ca. 0.5 M OH^-(e.g., simulated concrete pore solutions). The Ag/AgCl electrode in cement-based materials (mortar or concrete) has been used as an embedded reference probe for cathodic protection systems, where they showed good long-term stability over several years. However, the stability of Ag/AgCl electrodes was poor at very low chloride contents. While not disclosed here, some engineering improvements have been made to the custom-made Ag/AgCl electrode to improve its longevity as a chloride probe in concrete.

The Southwest Research Institute (SwRI®) patented MAS technology will be used to measure the corrosivity of the local environment in concrete. Instead of directly measuring the corrosion rate of the actual rebar embedded in concrete, the MAS measures the instantaneous corrosion rate of multiple miniature electrodes (~1 mm in diameter) made of the rebar material. It should be noted that changes in the corrosion characterization of rebar material can be considered negligible, independent of the alloying elements in the rebar material. In other words, the use of MAS sensors is intended to capture dramatic changes in the instantaneous corrosion rate, instead of incremental changes. The MAS sensor will be less than 1 cm in diameter, with 9-pin electrodes sealed in an inert epoxy matrix, as shown in Figure 2 (which however has 16-pin electrodes). With careful fabrication of the MAS sensor, the risk of crevice corrosion has been eliminated, as indicated by the SwRI seed grant research results.
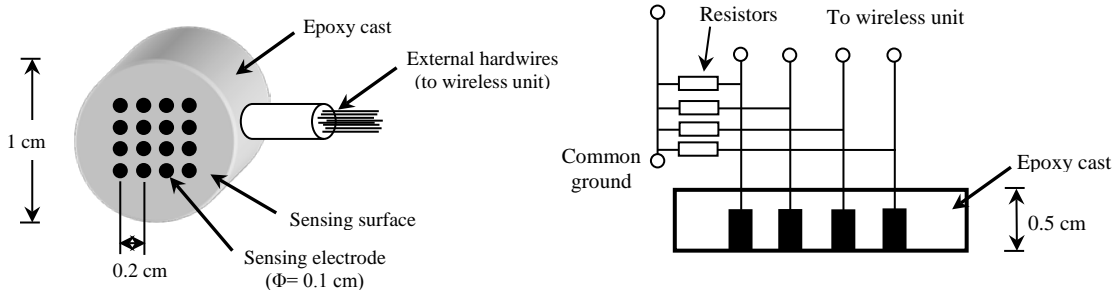
Figure 2. Schematic representation of a 16-pin MAS probe

The small pins are coupled together by connecting each of them to a common ground through independent resistors. The coupled MAS pins conduct corrosion current measurements by reading the differential voltage across precision 100 Ω resistors. The resistors are connected in a series chain, each connection mode being a port to an electrode of a corrosion probe array. In this manner, currents originating from an individual pin can be measured in sequence. In a corroding environment, anodic currents flow in the more

corroding pins (anodes) and the counteracting cathodic currents flow out of the less corroding pins (called cathodes). The MAS is suitable to measure corrosion rates in non-uniform corrosion processes where the electrochemical reactions may differ on the different pins (electrodes). As a result, each pin would develop its own electrochemical potential and current. The total anodic corrosion current may be expressed as:

$$I_a = I_a^t + I_a^c \qquad (1)$$

where I_a^t is the external anodic current that flows between pins (electrodes) and I_a^c is the internal anodic current that flows from the cathodic sites within each pin (electrode). To measure I_a, the coupled MAS relies on the measurement of I_a^t. The internal current I_a^c cannot be directly measured but is small enough to be ignored for small diameter electrodes. The current density so measured is utilized as the corrosion signal since it is proportional to the corrosion rate of the metal.

1.3. Study Objectives

The goal of this research is to develop a reliable, cost-effective corrosion monitoring system for existing DOT RC structures. To this end, the research objectives include: 1) improving and validating the SwRI corrosion sensor prototype for use in the concrete corrosion monitoring system; 2) developing algorithms for quality control and interpretation of the sensor data; 3) making viable recommendations to implement the corrosion monitoring system for existing DOT inventories of RC bridges; and 4) delivering a deployable prototype corrosion sensing system for DOTs to continue field evaluations.

As sensors become ubiquitous in engineering systems, this research, if successful, would add value to and leverage the success of ODOT and AKDOT & PF's recent deployment of structural health monitoring on select bridges. We envision the corrosion monitoring system to include: 1) an integrated sensor that can be easily embedded into existing RC structures and *in situ* monitoring of localized chloride content profiles and corrosivity (using SwRI-patented MAS technology); 2) a web-based wireless data communication and acquisition system; and 3) a software program that interrogates the collected sensor data for quality control (QC) and corrosion risk assessment. The sensor data will be automatically and periodically obtained to shed light on the risk of rebar corrosion and the health of the concrete. Data will ultimately be fed into the software program and presented via a user-friendly interface. The overall system will provide critical, actionable information and facilitate asset management and decision-making related to infrastructure maintenance and rehabilitation. The key innovation in this research lies in the holistic, integrated approach to rebar corrosion monitoring. Structural health prognosis, made possible by the use of multiple, miniature sensors embedded in aged structures, will provide a means to analyze the current state of corrosion and possibly predict when maintenance actions will need to be performed.

1.4. Research Approach

Task 1. Improving sensor system prototype and benchmark testing in the laboratory

The focus of this task is to configure the sensors for use in bridge structures and integrate the sensors with a wireless sensor platform. With a SwRI seed grant, a sensor prototype has been

developed with probes for chloride concentration ([Cl-]), pH, corrosion risk (MAS probe), and concrete resistivity, and a reference probe aligned in a 1½″ × ¾″ polyacrylate cylinder mold (Figure 3). A ribbon connector was used to connect the individual transducers to the wireless sensor platform.

In this task, a prototype of the reconfigured corrosion sensor will be fabricated and benchmark parameter calibration testing will be conducted. As such, this task will:

(1) Modify sensor configuration (eliminate the concrete resistivity and pH probes, extend the chloride sensing unit into a sensor array) such that the most valuable data parameters are acquired;
(2) Select sensor housing materials and optimize sensor alignment to make it suitable to be embedded into both new and existing RC structures;
(3) Improve the fabrication of chloride probes for better longevity in concrete;
(4) Modify platform configuration to be compatible with new sensor configuration;
(5) Validate the modified sensor system and calibrate its performance.
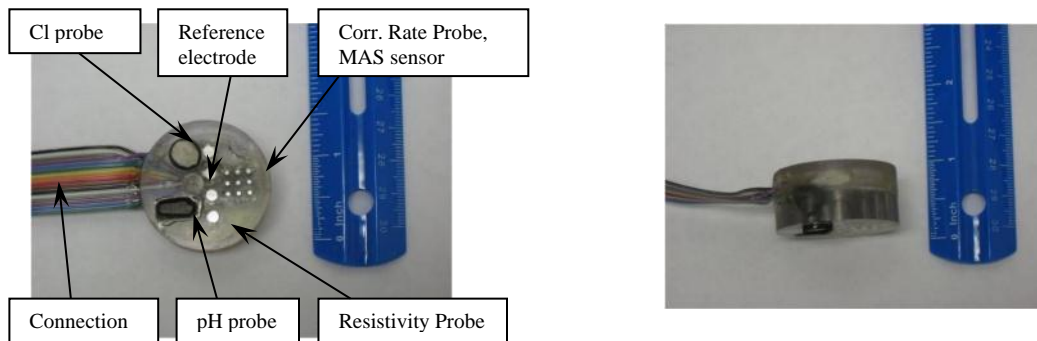
Figure 3. Prototype sensor configuration and profile.

Task 2. Testing sensor longevity and validating embedment method

The focus of this task is to test the longevity and reliability of the critical sensing elements in the proposed system and to develop and validate an embedment method that does not significantly compromise the local environment in the concrete to be monitored.

The long-term integrity and stability of the MAS probe, chloride probes and reference probes integrated into one sensor are critical to the success of this project and to the success of the proposed sensing system for their practical application in ODOT concrete structures. As such, they will be evaluated in an accelerated manner, by regulating the critical environmental variables (e.g., alkalinity, chloride concentration, heat, and moisture) during controlled "weathering tests". The weathering tests will subject the integrated sensor to a cyclic procedure of immersion in simulated concrete pore solutions (0.6M KOH + 0.2 M NaOH + 0.001 M $Ca(OH)_2$) with a given NaCl concentration for two weeks at 104ºF (40ºC) and subsequent drying by air for 3 days at room temperature. In the first four cycles, the hours of wetness will have the NaCl concentration increases from 0.001 M, to 0.01 M, 0.02 M, and ultimately 0.03 M. This will be followed by another four cycles, where the hours of wetness will have the NaCl concentration increases from 0.04 M, to 0.06 M, 0.08 M, and ultimately 0.10 M.

During the hours of wetness, the sensing elements will be connected to the data acquisition system and their readings will be taken at least on an hourly basis to monitor their stability during the immersion time and as a function of wetting cycle. The sensitivity and error levels of each sensing element will be analyzed as data become available.

Before and after each weathering cycle, the potentiometric response of the Ag/AgCl electrodes will be measured in saturated $Ca(OH)_2$ solutions simulating the concrete pore solution contaminated by free Cl^- concentration ranging from 1×10^{-4} to 2 M to see whether they still maintain good linearity with the logarithm of the Cl^- concentrations.

Similarly, the potentiometric response of the reference probe in the sensing system will be measured against that of a reference electrode that did not undergo the weathering tests. The purpose of this test is to determine whether they are prone to the exposure to various solutions, heating or wet/dry cycling.

The corrosion rate of the MAS probe will be measured against that of three bare steel rebars that also underwent the weathering tests. This will be done to ensure that MAS results are consistent with the corrosion rate of rebar (measured via electrochemical impedance spectroscopy - EIS).

During this task, the optimal method of embedding the integrated sensor into existing RC structures will also be finalized. The sensor embedment method will be designed to best capture the possible two-dimensional diffusion of water and chlorides seen in ODOT bridge girders (see Figure 1).

Task 3. *Demonstrating pilot-scale system in the laboratory and establishing guidelines for sensor implementation at existing RC structures*

The objective of this task is to conduct a pilot-scale test in the laboratory and establish guidelines for sensor implementation at existing RC structures. We will demonstrate the pilot-scale system in the laboratory to test and validate the performance of the overall sensing system. Continuous monitoring for extended periods will provide valuable information regarding the reliability and durability of the sensors. A combination of multiple sensors enables proper calibration of on-site measurements, whereas readings over time make it possible to assess the transport properties of chloride ions and to monitor the corrosion behavior of the reinforcing steel. As such, this task will deliver a calibrated, integrated multi-parameter sensor for further field evaluation. The laboratory testing results will be used to establish guidelines for the sensor implementation at existing RC structures.

Task 4. *Developing methodology for sensor data QC and interpretation*

Data mining coupled with on-site sensor measurements provides a powerful tool for recognizing corrosion patterns as they unfold in real time and provides valuable insights on corrosion initiation and propagation and structural degradation. This task will develop the method and a software program to display and interrogate the collected sensor data. The actionable corrosion condition information will be presented through an intuitive interface to facilitate asset management and decision-making by ODOT personnel.

To minimize the interference inherent in sensor noise, we will reject sensor readings that are apparently false and filter/condense the sensor readings as necessary. Thereafter, a methodology will be developed and refined for QC/outlier detection of each sensing element in the corrosion sensing system.

The chloride concentration profile at time t is obtained by the three chloride probes embedded at different depth of the concrete. Such data will be periodically used to evaluate the remaining service life of the concrete structure. This is based on the assumption that once sufficient chlorides accumulate on the rebar surface, it will initiate the active corrosion of the rebar and the time for corrosion initiation is much greater than the time for corrosion propagation to failure.

Ultimately, we expect that the numerous periodical measurements of corrosion and environmental parameters inside the concrete will provide: (1) abundant data to develop the algorithms for data display and QC; (2) capability of an evolving predictive model that can capture the near-real-time condition of the structure being monitored and adapt to sudden degradation of rebar and/or service conditions during extreme events (e.g., earthquake).

Task 5. Demonstrating the pilot-scale system in the field

This task will test and validate the performance of the overall corrosion monitoring system (including both hardware and software) in the field. The bottom of a girder on a select ODOT bridge will be used for the field testing, as described in the problem statement section. As such, the developed sensing system will be deployed in an aging ODOT RC structure in the actual coastal environment. To place the sensor in the existing RC structure, cores, the same size as the sensor jacket tube, will be extracted from the chosen exposure environment. The integrated sensor will then be embedded in concrete following the guideline established in Task 3. The electronics package will be placed at a convenient location on the outside of the column. The response of all probes within sensors will be monitored periodically. Data analysis will be performed at the web portal.

Note that the research team has coordinated extensively with ODOT and AKDOT & PF about this task. The field deployment of the pilot-scale system in a select ODOT bridge girder (Pier 1 at the north end of the Yaquina Bay Bridge) will occur in the first month of 2013, after which monthly data collection will be conducted by ODOT and the collected data will be fed into the software developed in Task 4 for analysis. Current ODOT practice generally involves concrete coring at four select locations on each bridge. At each location, three cores are obtained for enhanced data reliability. Thereafter, each obtained concrete core is assessed in the laboratory for its chloride content at every 1/2″ of depth down to 2″. The field deployment task will also shed light on the number of sensors and appropriate configurations needed to achieve a systematic understanding of the corrosion condition for an entire ODOT RC structure. A sampling approach may derive from the improved understanding gained from this task.

In light of various challenges identified for deploying such a system in Alaska, another agency is being sought as an alternative to AKDOT & PF for demonstrating this system in the field.

CHAPTER 2 – FINDINGS

2.1. Improving the Corrosion Sensor System

2.1.1. Developing New Sensor Prototype

The proposed corrosion sensor is based on the corrosion sensor developed and patented by SwRI, in which a 9-pin MAS corrosion current sensor, an Ag/AgCl chloride probe, a mixed metallic oxide (MMO) pH probe and a four-point concrete resistivity probe are included in each sensor unit. This sensor is capable of monitoring rebar corrosion current, chloride content, concrete pH and resistance *in situ*. According to ODOT's advice, the fluctuations in the pH and resistance of bridge concrete structures are not very significant and thus are not considered as the key issues for rebar corrosion and concrete degradation. Therefore, the MMO and concrete resistivity probes in the prototype were removed from the new sensor prototype. Furthermore, ODOT indicated that the lower corners (at the side) of a bridge girder are the most severely corroded areas. This can be attributed to the ingress of chloride anion (Cl$^-$) into the concrete through both the side and the lower surfaces of each corner. The new sensor prototype should achieve valuable information from both directions to evaluate and predict corrosion progress of rebar and ultimately the degradation of the structure. In this context, the proposed sensor prototype involving an array of sensor units has been designed and shown in Figure 4.
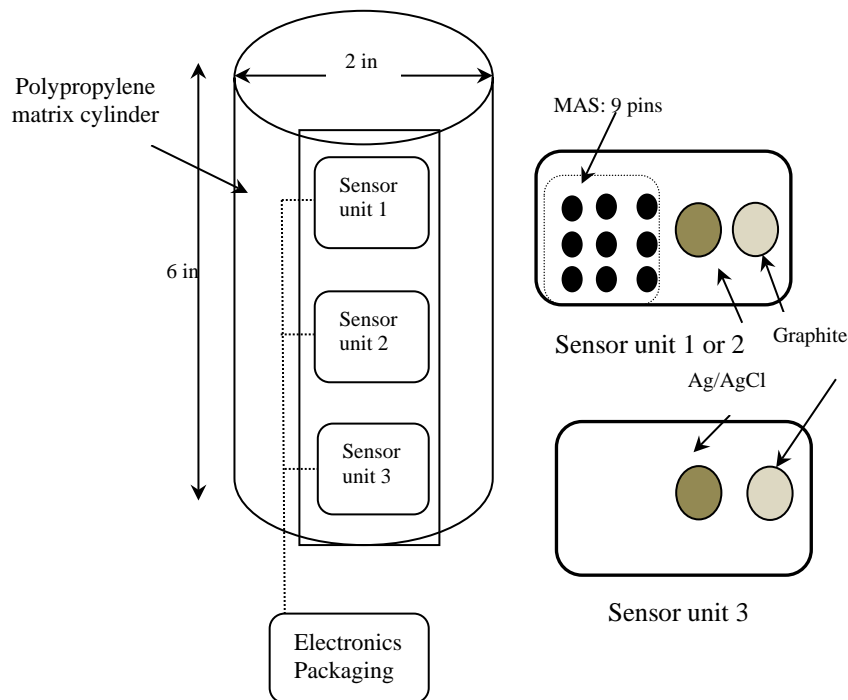
Figure 4. Proposed new sensor prototype

16

The rebar at the sensor unit 2 location might experience the most severe corrosion attack under the girder environment in Oregon (see Figure 1), whereas the sensor units 1 and 3 in this prototype shall be able to monitor the two-directional ingress of chloride from environments outside the girder.

2.1.2. Improving Ag/AgCl probe

The existing research indicates that while Ag/AgCl remains sensitive to chloride content variation in highly alkaline concrete environment, its long-term durability as a chloride probe is a key concern as the sensing surface layer gets oxidized by the hydroxyls in the concrete pore solution.

The conventional Ag/AgCl probe fabrication process involves dipping an Ag rod into a molter bath of AgCl to develop a thick AgCl coating, as shown in Figure 5a. One disadvantage for this approach is that the contact area between the Ag rod and AgCl coating is a relatively small flat surface which may facilitate the oxidation of the Ag/AgCl interface by hydroxyl ions at a relative rapid rate. Based on field experience, a greater Ag and AgCl contact area or a more complex Ag/AgCl probe geometry can effectively improve longevity of the probe in high-alkalinity environments. A possible explanation is that the greater contact area or complicated Ag/AgCl probe geometry increases the time required for the hydroxyl ions to oxidize the silver at the Ag/AgCl interface, thus delaying its degradation as a chloride probe.

(a)   (b)
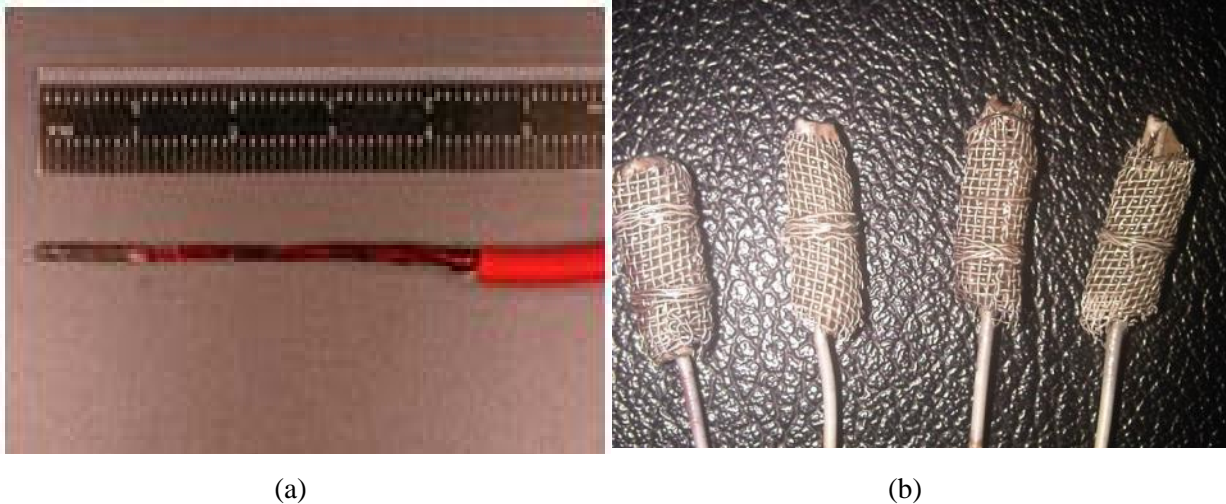
Figure 5. Ag/AgCl probe with different fabrication approaches: (a) conventional and (b) current.

In this context, the fabrication process was improved at SwRI and described as follows. After dipping the Ag rod into molten AgCl twice, a #20 Ag mesh (diameter: 0.04 in) was wrapped on the AgCl coating surface. Subsequently, the whole probe pack was dipped into the molten AgCl to promote a light AgCl coating on the surface of the mesh. Subsequently, the electrical connection between the Ag wire and mesh was checked. This new process can partially re-melt the AgCl packed between the Ag mesh and rod and result in a more compact bond between the Ag/AgCl mesh and Ag/AgCl wire with a larger contact area. For comparison, the Ag/AgCl probe fabricated using this process is shown in Figure 5b and the probe fabricated using the conventional process is shown in Figure 5a. This new approach

builds a good Ag/AgCl bond and provides a more stable electrode potential (Ag/AgCl) for a relatively long time.

Alternatively, experiments were conducted at the WTI's Corrosion & Sustainable Infrastructure Laboratory (CSIL) to fabricate 18 different Ag/AgCl probes by first electrodepositing AgCl onto Ag rods and then soaking the Ag/AgCl into a certain polymeric solutions for a given time. At each step of the fabrication process, an Olympus BX61 optical microscope was employed to examine the surface morphology of the prepared sensing surface, as illustrated in Figure 6. Once each probe was made, its potentiometric response was measured in five simulated concrete pore solution with varying chloride concentrations; and the data all showed very strong linear correlation between the open circuit potential of the probe and the logarithm of chloride concentration (with R-square no less than 0.96). A Ag/AgCl probe made with electrodeposition but not followed by dip-coating was used as a control, for the probe longevity testing described in a later section.

(a)	(b)

| (c) | (d) |
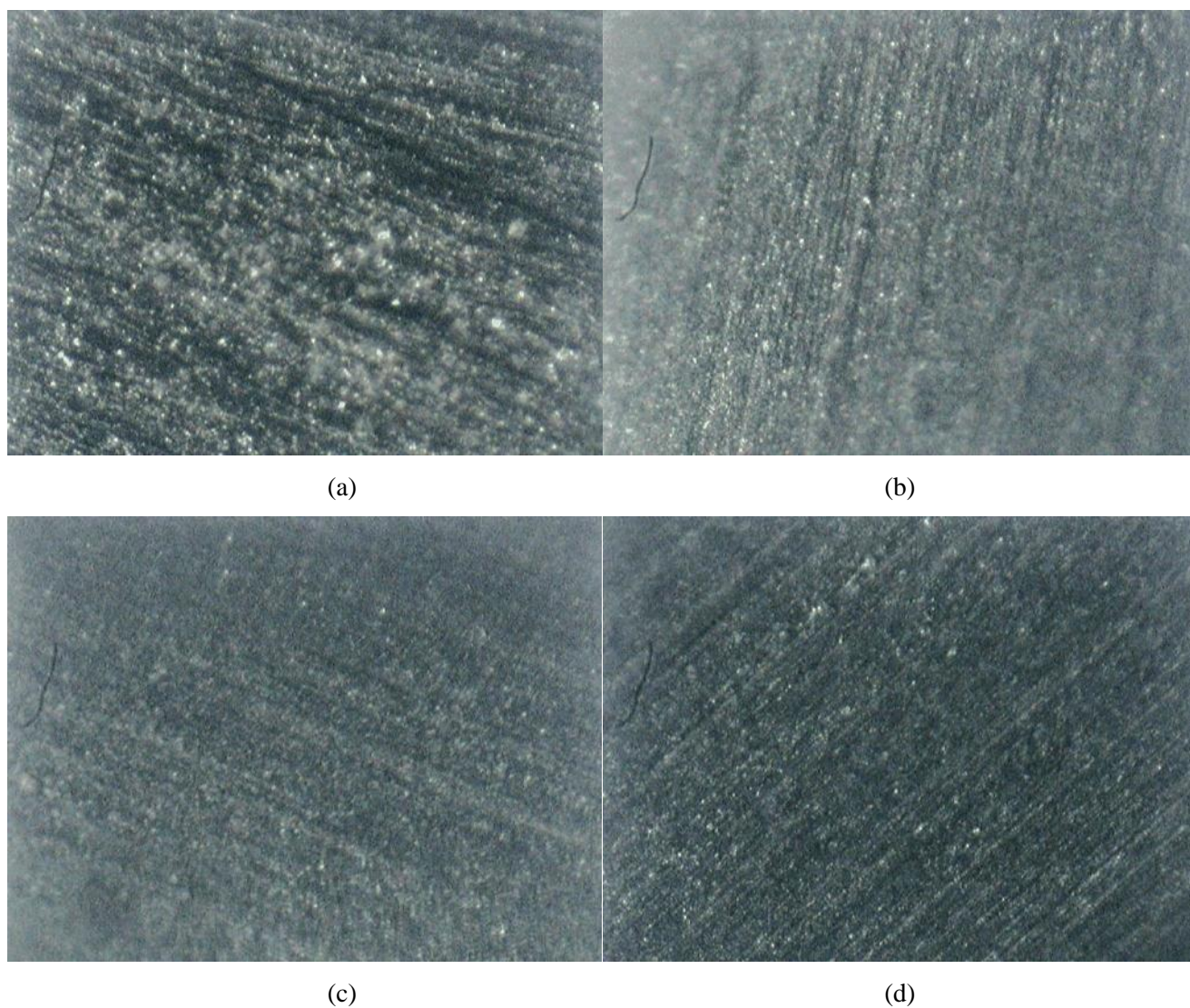
Figure 6. Micrograph of Ag/AgCl probe surface after various stages of (a) to (c): electrodeposition and (d): polymeric coating.

2.1.3. Building the New Sensor Prototype

A total of four proposed sensor systems were built in this project. The first two systems are of the version being used in the SwRI laboratory tests for calibrating and benchmark testing and in the WTI CSIL for sensor longevity testing. Their fabricating process is described in this section. The last two systems were built with minor modifications to the previous version in light of the laboratory test results and were delivered to ODOT and a yet-to-be-determined agency for field implementation. The minor modifications focused on the addition of a temperature sensor and changes to the wire connection and board configuration.

The fabrication process of sensor body is described as follows. As schematically illustration in Figure 4, polypropylene has been selected as the matrix material for the sensor fabrication. Polypropylene material exhibits excellent chemical resistance, robustness in concrete structures, machinability and ease in setup of the sensor probes. A cylinder with a diameter of 2 inches and length of 6 inches was machined. A port with a ½ inch diameter was hollowed out in the center from one end of the cylinder. Subsequently, the cylinder was sliced into two halves along the longitude direction. A 1/8 in depth slice parallel to the sliced surface was cut on one half for the probe layout and installation. Holes for the probe layout were drilled on the sliced surface according to the design geometry. The diameter of holes for the Ag/AgCl and graphite probes is ½ inch and set adjacent to the 9-pin MAS probes. The holes for the MAS probe are 0.05 in diameter and 0.1 inch in length from pin center to center.

The material and size of sensing probes were prepared according to the design requirements. Figure 7a shows the photograph of the Ag/AgCl and graphite probes made for the sensor. A high-density graphite rod was used to serve as the reference electrode in concrete. The geometry of both probes is ¼" in diameter with a length of ½". An electrical wire was spot welded on the base of the Ag rod of the Ag/AgCl probe and then glued and sealed with conductive epoxy. The graphite probe was connected with a wire at the rear surface with conductive epoxy. The material used for the MAS sensing probes was a 1018 carbon steel wire with a diameter and length of 0.05 and ¼ inches, respectively. The probes were spot welded with electrical wire opposite of the sensing surface. All the probes were inserted into the designated holes after being coated with epoxy on the non-sensing surfaces. The coating facilitates affixing the probe in the hole and avoids humidity ingress into the electrical connection location. The epoxy seal on the MAS probes avoids crevicing between the probes. Epoxy was poured into the hollow tube port to seal the wire connections at the rear end of the probes. The photograph for the rear wire connection and epoxy seal is shown in Figure 7b.

The top-view photograph of the sensor prototype and the overview of the wired sensor are shown in Figure 7c and 7d, respectively. The sensing surfaces of the MAS and graphite probes were polished to a #600 grit surface finish. The surface of the Ag/AgCl probes were indented 0.05 inch into the matrix. A 24 pin standard serial cable was used to electrically connect the MAS probes and ribbon cables were used to connect the graphite and Ag/AgCl probes to the electrical platform. The electrical connection of all the probes was examined after the assembly.
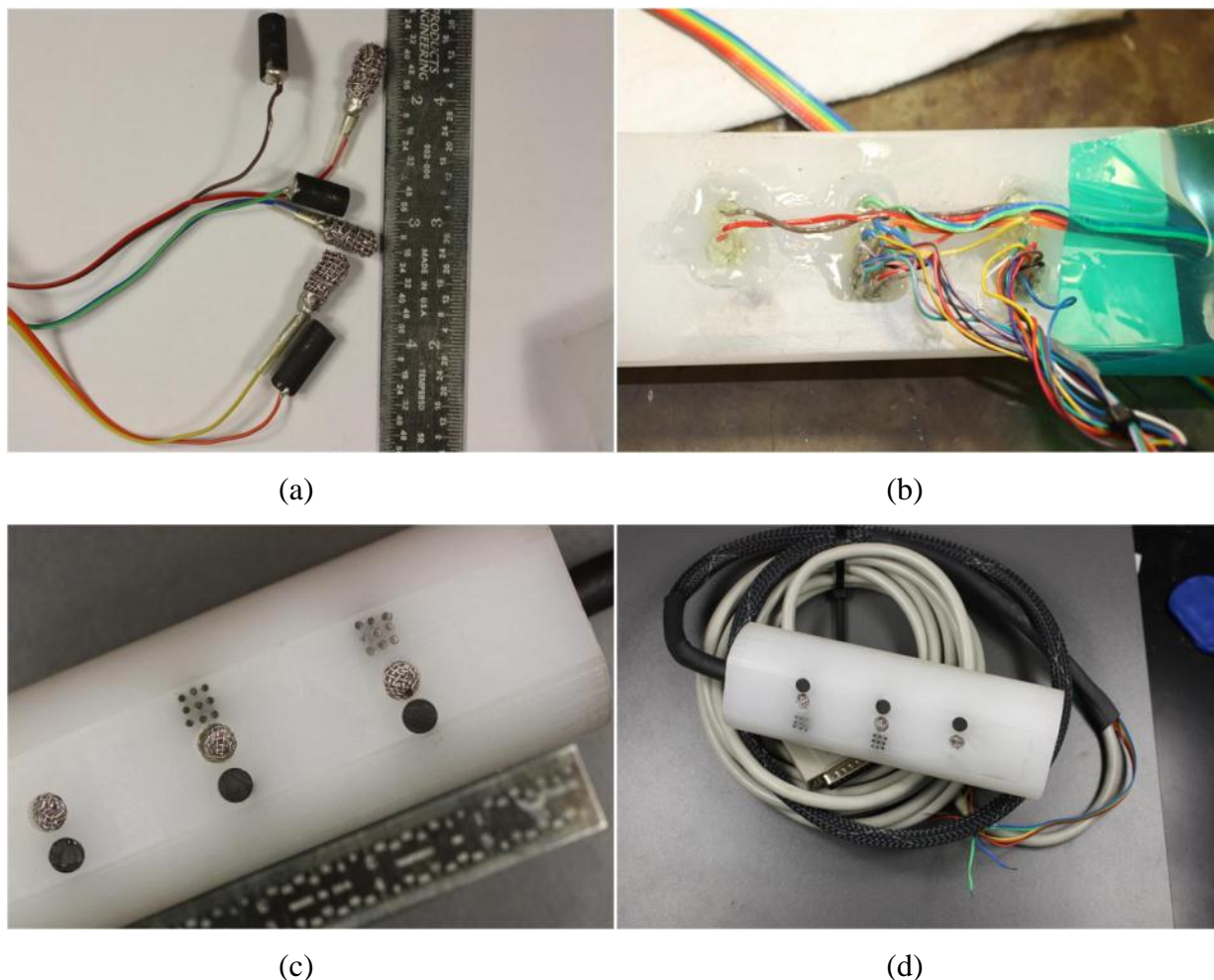
Figure 7. (a) Ag/AgCl and graphite probes, (b) wire connection inside the sensor tube, (c) top-view photograph of the sensor prototype, and (d) sensor and wired cable.

2.1.4. Building the New Sensor Platform

This part of work is based on a previous sensor platform developed by SwRI and Aginova Inc. The new sensor platform and the demo sensor system are shown in Figure 8. In this platform, a 16-wire MAS sensor data acquisition and communication board (shown in Figure 8a) and two sets of potential data acquisition and communication boards (shown in Figure 8a) are included. The MAS board wire connects to the sensor through a military connector (shown in Figure 8a). In future laboratory studies, the 16-wire MAS sensor board will be separated into two 8-wire groups and each group will connect to 8 of 9 pins in one MAS sensor (shown in Figure 4a). The last pin in the 9 pin MAS sensor will be used to make a potential measurement reading or as a backup for the 8 pins. When data are transmitted to the PC data interface, the corrosion current from the 8 pins will be shown separately, in a table and plotted as necessary. Also shown in the table are the maximum and average anodic current from the 8 pins (i.e., ΔI_{ij}).
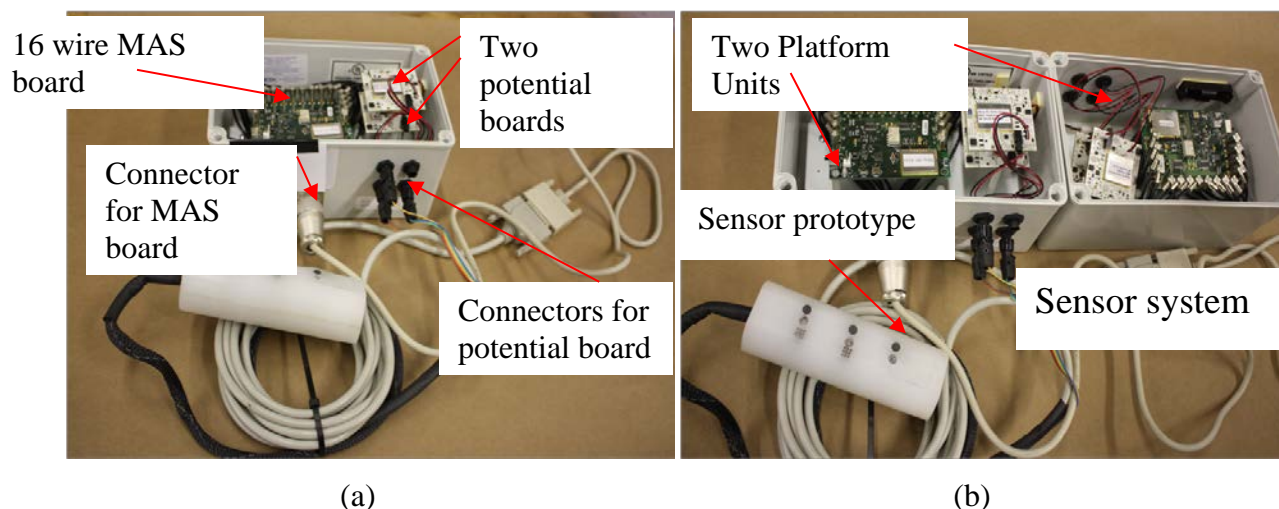
Figure 8. Sensor data acquisition and communication platform unit (a) and the overall sensor system (b)

2.1.5 Web-based Wireless System and Specifications

The built platform uses a web-based wireless system with a low-power onboard processor for continuous data acquisition. Based on the previous work on continuous corrosion monitoring using low-power wireless corrosion sensors conducted for the U.S. Marine Corps and U.S. Army by SwRI and Aginova, the MAS, chloride and reference probe technology will be integrated into the functional and existing wireless sensor platform that transmit corrosion data through a low-power Wi-Fi transceiver with an ARM processor. The transceiver and detail parameters are depicted in Figure 9.

An advantage of the adopted Wi-Fi based communication system is its ability to use off-the-shelf routers, thereby eliminating a significant development and implementation cost required for specialized Zigbee based systems. Another advantage is the use of state-of-the-art data encryption technology for security. Within the current platform system, a wireless gateway for sensor data collection, a web-based portal that uses web services, and a XML-RPC layer that communicates between the gateway and the portal (for storing data in databases) can be viewed using a browser that has been installed at SwRI. The data acquisition unit is hermetically packaged and capable of functioning over a wide temperature range for up to 3 years without replacing the single 3.6 V Li AA battery powering the units while making measurements every minute.

Laboratory experiments were conducted at SwRI to test the built platform and calibrate the sensor probes, the results of which were satisfactory.
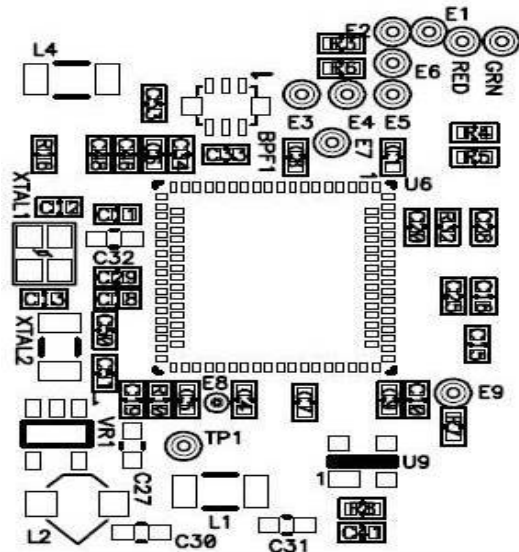
Application Processor	32-bit MCU Operating @ 44 MHz
Data Rate	Up to 2 Mbs
Radio Protocol	IEEE 802.11b/g compatible
Standards	IEEE 802.11, 802.11i,k,e,d; IEEE 1588
Security (802.11i)	WPA2, AES Encryption, EAP-FAST Authentication
I/O	GPIO, UART, 10-bit ADC

(a)   (b)

Figure 9. (a) Schematic for the Wi-Fi wireless transceiver with an ARM processor, (b) Specifications of the communication module

2.2. Calibrating the Sensor Probes and Benchmark Testing in the Lab

The objectives of this test are to 1) calibrate probes in the sensor, 2) conduct the benchmark test, and 3) evaluate the system performance. Figure 10 shows the detailed test setup for the calibration and benchmark testing at SwRI. This test was conducted in a representative simulated pore concrete solution SPS1 (pH= 13.3). Before the test, the sensor body was wire connected to the platform, the platform was synchronized with the router, the software was installed into a laboratory PC and the data acquisition frequency was prioritized. In the beginning of this test, the sensor was placed in the SPS1 solution for two weeks with no chloride added. Subsequently, sodium chloride crystals were added to the solution periodically (every three to four days) to achieve the designated chloride concentration until the final concentration reached 1 mol/L. The increase of chloride content in the solution was stepwise.
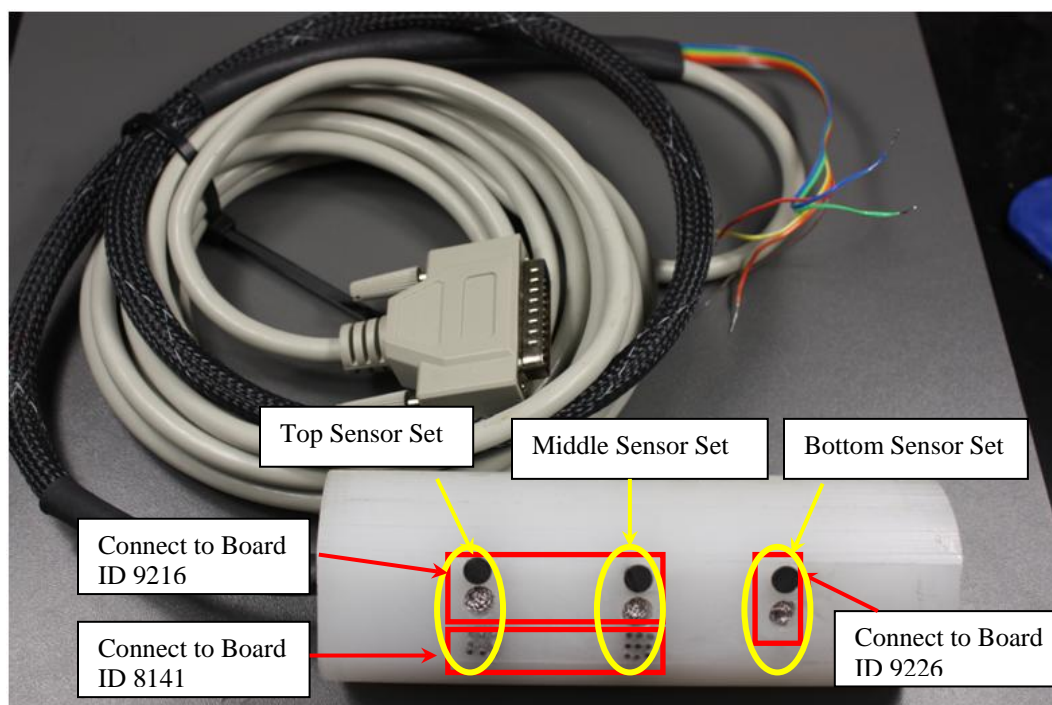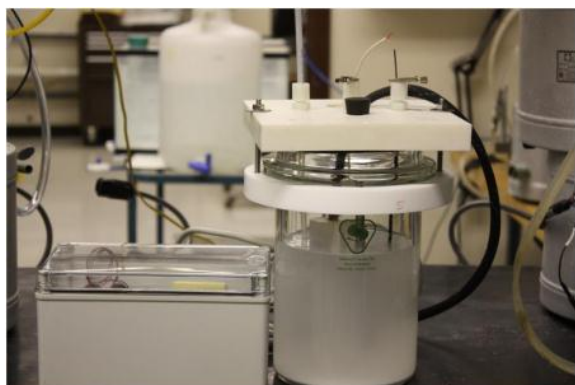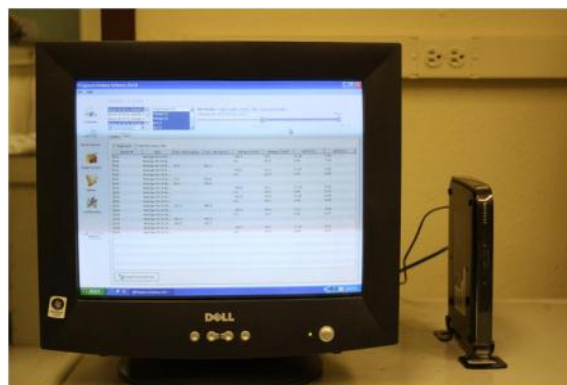
Figure 10. Sensor and the setup of the sensor calibration test (a) close up picture of the multi-probe sensor (b) test cell and platform unit (c) router and laptop (software interface)

During the test, all probes within the sensor body were completely immersed in the solution, along with a conventional three-electrode Linear Polarization Resistance (LPR) test system. The system included a carbon steel rebar (#5 and 4″ length), a saturated calomel electrode (SCE) and a platinum mesh counter electrode for electrochemical measurements. The three-electrode system in the test solution was employed to acquire the rebar corrosion rate at a certain time interval, using the LPR technique. The LPR measurements were conducted immediately prior to every incremental chloride addition into the test solution. The acquired rebar corrosion rate was compared with the corrosion rate from MAS probe within the same time frame to correct and calibrate the MAS data.

Nitrogen was first purged into the solution to eliminate or minimize the effects of carbonation on the solution pH. The nitrogen purging continued for one week and then was stopped. The pH of the test solution was measured periodically to monitor any fluctuations produced by the addition of chloride. The results indicate that pH fluctuations within the overall test duration were less than 0.2. The effects of this small variation of pH on potential and corrosion rate readings are considered negligible.

Within the test duration, three sets of data are shown on the software interface including: average corrosion rate (average of 16 pins), maximum corrosion rate (the corrosion rate of an individual pin with the most aggressive corrosion) and potential readings from three chloride probes. Note that eight of nine pins for two MAS probes (in the top and middle sets of the sensor configuration as shown in Figure 10a) were connected to the MAS board (ID:8141). Therefore, the maximum and average corrosion rate in this study represents the results of the 16 pins of two MAS probes but not the corrosion rate of one individual MAS probe. This setup is due to the lack of electronics boards. The No.9 pin in both MAS probes were insulated and not connected to the MAS board. On the other hand, the sensor was immersed in the homogeneous testing solution, in which the corrosion rate of the two 9-pin MAS probes should be identical. Therefore, in this calibration and benchmark test, we did not differentiate the corrosion rates of the two MAS probes. The plots of all three sets of data can be shown directly as function of time in the software program. The test cell and the sensor platform are set up on a laboratory bench more than 10 feet from the router and laptop in another room. The test lasted for approximately 8 weeks.

The raw testing results were exported into EXCEL and then plotted as shown in Figures 11-13. Figure 11a, 12a, and 13a show, respectively, potential readings of top, middle and bottom chloride probe in the sensor as a function of elapsed time and [Cl⁻] variation in the SPS1 solution. Correspondingly, Figure 11b, 12b, and 13b show the relationship between the logarithmic chloride concentration and the probe potential readings. The results in Figure 11a, 12a, and 13a indicate that all chloride probe potential readings were sensitive to chloride concentration variation from 0.0001 to 1.0 mol/L. The potential readings stayed relatively stable at each specific chloride concentration and abruptly shifted in the positive direction once additional chloride was added into the solution.

From Figures 11a, 12a, and 13a, there are several anomalous observations. First, at the beginning of the test, the potential (vs. graphite reference electrode) of the middle and bottom chloride probes shifted abruptly in the negative direction before chloride addition. Such shift did not occur to the top chloride probe (Figure 11a), the potential of which was relatively stable (-260±20mV vs. graphite) from the beginning of when the probe was immersed into the solution to the first chloride addition. All probes were carefully cleaned with de-ionized (DI) water before being immersed into the test cell. After the test, the surfaces of all chloride probes were carefully examined and no contamination or precipitation was found on the probe surfaces. The rapidly changing potential readings prior to chloride additions may be attributed to the electrochemical response time for the three probes (or the graphite reference) after being immersed in the high-alkalinity environment. This discrepancy may be minimized or totally eliminated by fabricating the probes using a consistent procedure. Under worst case conditions, a "break in" time may be required to allow for surface stabilization prior to the acquisition of accurate measurements.
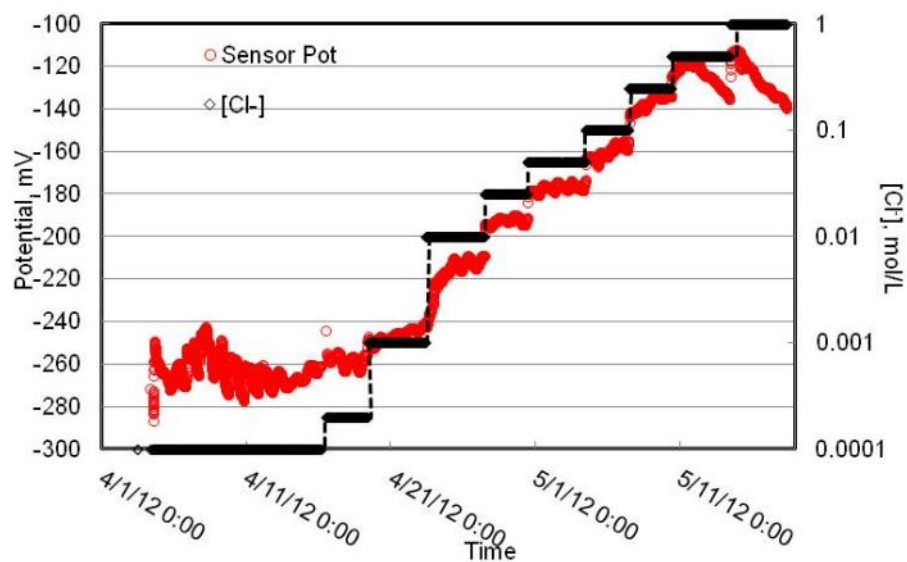
(a)
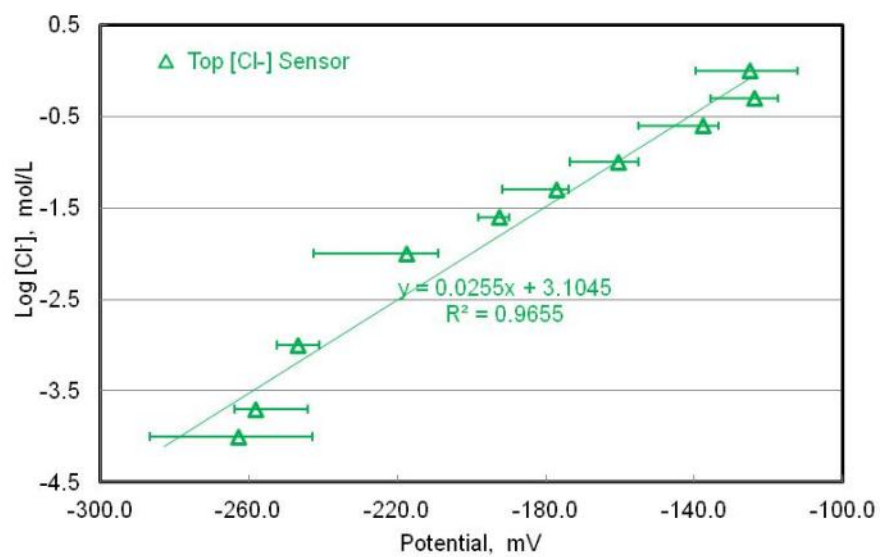
(b)

Figure 11. (a) Potential readings of top chloride probe as a function of [Cl$^-$] stepwise variation in SPS1 solution; (b) Chloride concentration vs. probe potential readings
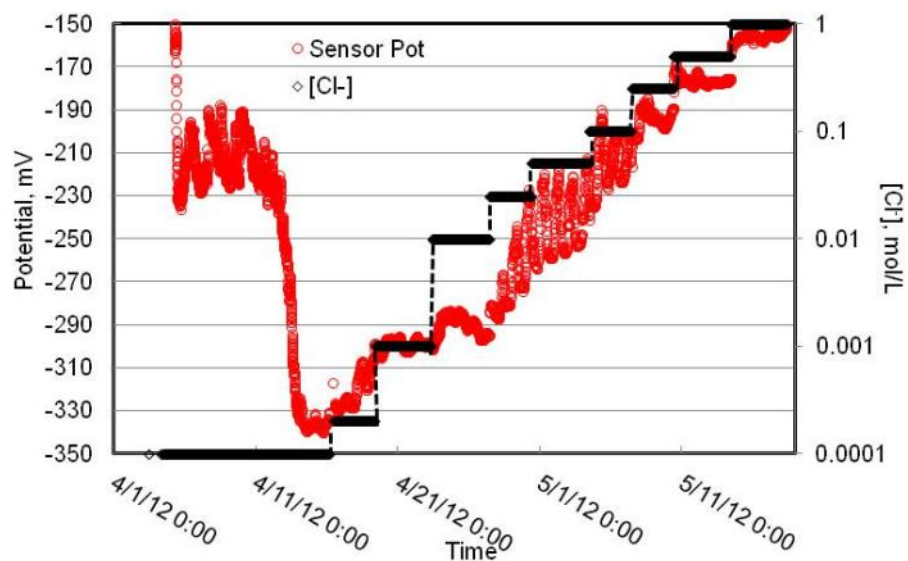
(a)
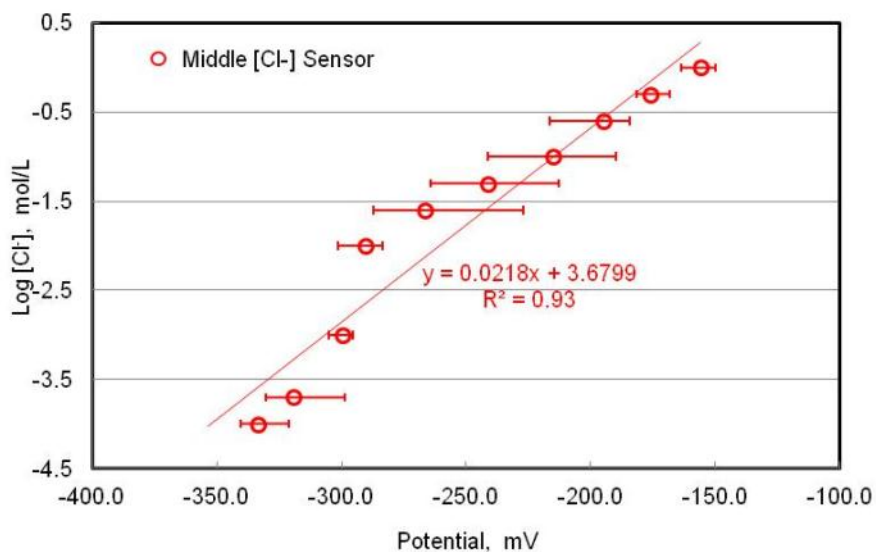
(b)

Figure 12. (a) Potential readings of middle chloride probe as a function of [Cl⁻] stepwise variation in SPS1 solution; (b) Chloride concentration vs. probe potential readings

26
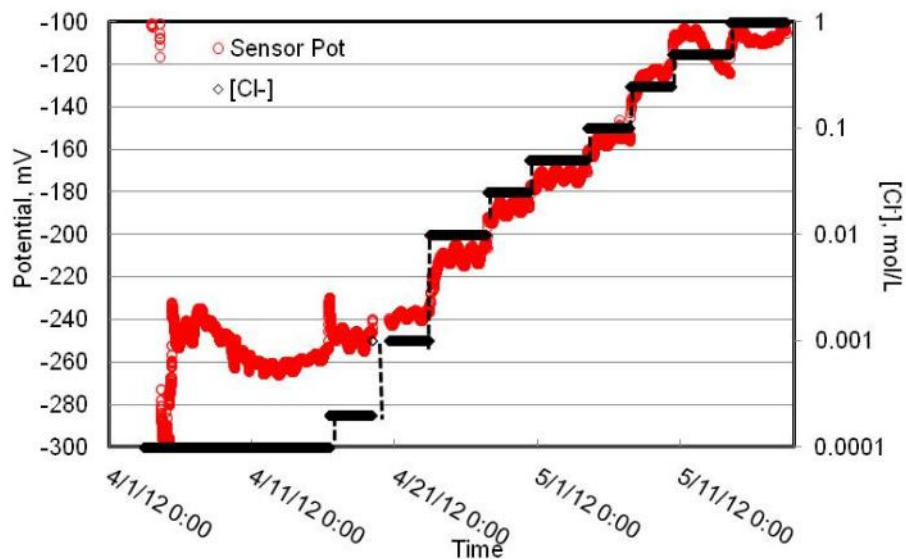
(a)
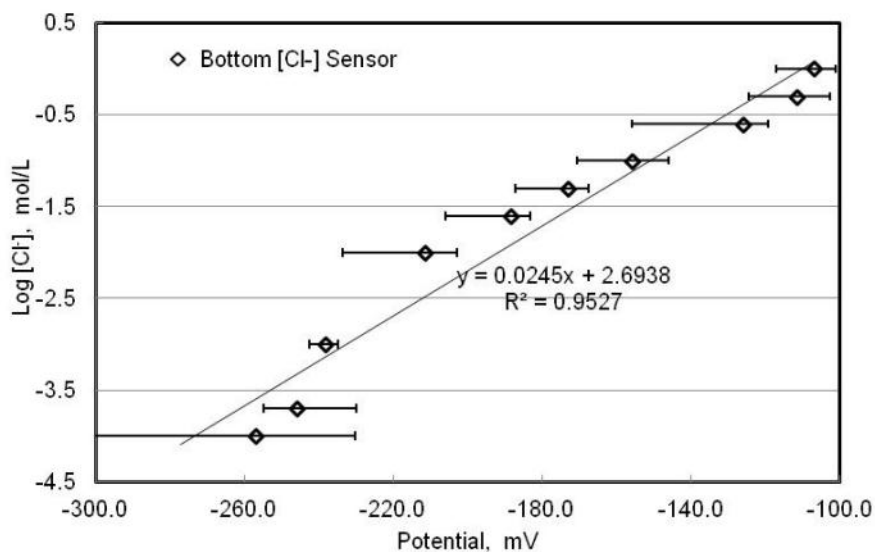
(b)

Figure 13. (a) Potential readings of bottom chloride probe as a function of [Cl⁻] stepwise variation in SPS1 solution; (b) Chloride concentration vs. probe potential readings

Another anomalous effect is that, for the middle chloride probe (Figure 12a), the potential readings fluctuated significantly within the chloride concentration range between 0.005 and 0.05 mol/L. This may be due to unexpected contamination, such as bubbles in the solution forming on the probe surface and interfering with the electrochemical equilibrium.

The last anomalous observation is that, at the higher chloride concentration level (≥ 0.5 mol/L), the potential readings abruptly moved to positive direction immediately after chloride addition and subsequently shifted in the negative direction. This was observed for

the top and bottom chloride probes (shown as Figure 11a and 13a). This effect may be induced by the impact of the high and heterogeneous chloride concentration at the probe surface immediately after chloride addition. As chloride diffused evenly in the test cell, the potential dropped gradually towards the negative direction. It is worthy to note that the interval of each chloride addition was only three to four days, which was short to reach an homogeneous solution without extra agitation, especially when high concentration of ions were added.

The anomalous observations in the preliminary calibration test will help us further enhance the probe fabrication procedure, improve the capability for data diagnosis, and provide valuable experience for the next phase.

Figure 11b, 12b, and 13b show the average of the potential readings at each chloride concentration level, with error bars indicated. The trend line, its linear equation, and R-square value are also shown in the Figures. Note the similarity in the slope of these curves indicating good reproducibility between the chloride probes. This calibration in simulated pore solution combined with the calibration in the paste specimen will be used to calculate [Cl^-] according to potential readings in field deployment. For instance, the sensor 1 features the following correlation:

$$\text{Log } [Cl^-] = 0.0255 * \text{potential} + 3.1045$$

Figure 14 shows the results of corrosion rate measured by the MAS and the rebar as a function of elapsed time and chloride concentration. Note that data during 4/16/2012 to 4/20/2012 were not collected, due to a board problem. Fortunately, this caused no significant impact on the general trend of corrosion rates. The results reveal that, for most data points, the maximum corrosion rate (red hollow DOTs) of MAS probe was greater than the average corrosion rate (green hollow DOTs). Values of the max rate / average rate provide insight into localized corrosion that occurs on steel in the SPS1 solution. For some data points, especially after 4/26/2012, parts of the maximum corrosion rate data are extremely low, shown as 0 in Figure 14. This is believed to be related to firmware issues with the sensor system. We will examine the MAS board to verify proper operation prior to future tests and field implementation. Also to be noted for the data presented in Figure 14 is that, corrosion area of the rebar used in the calculation of rates is an estimate based on visual observation.
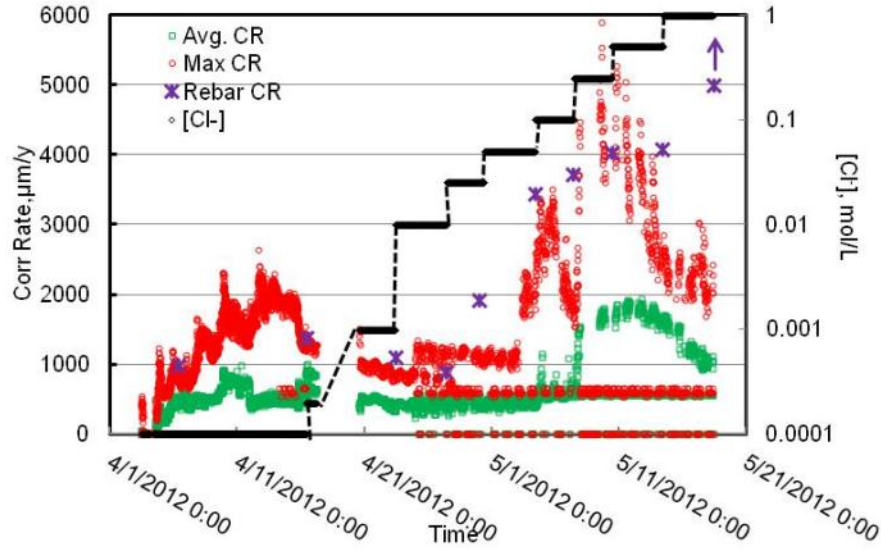
Figure 14. Corrosion rate, including maximum and average, results of MAS and rebar (by LPR) in SPS1 with stepwise incremental [Cl⁻].

The maximum and average corrosion rates from the MAS sensor and the corrosion rate from the rebar generally increased with the chloride addition. Both probes experienced passive to active corrosion transformation when the chloride concentration [Cl⁻] was in the range of 0.020 and 0.050 mol/L. Except for a few data points ([Cl⁻] at 0.025, 0.5 and 1.0 mol/L), the corrosion rates of the rebar were in reasonable agreement with the maximum corrosion rate readings of the MAS probe. This reveals that the MAS probe is a good tool to represent rebar corrosion rate in alkaline concrete environments with varying amounts of chloride present.

Corrosion initiation occurred when [Cl⁻] reached 0.05 mol/L and 0.025 mol/L for the MAS and rebar probe, respectively. Both of these two chloride concentrations fall in the range of threshold chloride concentration to initiate rebar corrosion discussed in literature. The discrepancy may be attributable to the significantly higher surface area of the rebar relative to the MAS probe. Statistically, greater surface exposure may induce the occurrence of localized corrosion earlier. Another possible explanation is the short time interval (three days) for the [Cl⁻] level at 0.025 mol/L. If as in the real world, the [Cl⁻] changes slowly and stays close to 0.025 mol/L for a longer duration, the active corrosion of MAS may occur at this chloride level as well. Actually, the active corrosion (abruptly increase in the maximum corrosion rate) of MAS probe occurred in the second day when [Cl⁻] level reached 0.050 mol/L.

At very high [Cl⁻] (0.5 and 1.0 mol/L), the MAS and rebar probes exhibited a reverse corrosion rate trend. In this chloride range, the corrosion rate of rebar increased with increasing chloride level but the corrosion rates of MAS (both maximum and average) decreased with the increasing chloride level. This is because corrosion products adhered to the MAS pin surface and acted to suppress the corrosion rates. For the rebar probe, new corrosion spots continuously emerged on the rebar surface resulting in further corrosion processes. In other words, *once active corrosion is initiated and a great amount of chloride is*

29

present, the MAS probe may no longer serve as a good tool to predict the corrosion rate of rebar unless more research is conducted to establish such prediction or correlation.

2.3. Demonstrating the Pilot-Scale System in the Lab

The objectives of this test are to: 1) exam the sensitivity of sensor probes to chloride ion variation inside a paste specimen and validate the preceding probe calibration results and 2) further evaluate the performance of the sensor system when embedded in a paste specimen. To reduce the test duration, a modified specimen configuration and test protocol were adopted for this test, as described below.

2.3.1 Fabricating the Paste Specimen with Sensor Embedded

Figure 15 photographically illustrates the paste specimen fabrication and curing process with consecutive pictures. The whole paste specimen was made of three layers with different cementitious materials and chloride concentration addition. The mix design is shown in Table 1. As shown in Figure 15a, a stainless steel mesh (6″ diameter) was placed at the bottom of the specimen to facilitate the later application of an electric field across the fabricated specimen. In the middle and top layers, there was a well-polished rebar with a 6″ length inserted into the paste and at the same height as the corresponding probe set.

Table 1. Mix design for the three paste layers.

Paste	Water/ Cement	Water, g	NaCl, g	Chloride Concentration, mol/L	Cement, g	Height in the container, in
Bottom	2/5	600	0.700	0.01	1500[*]	2 ½
Middle	1/3	500	2.925	0.1	1500 (Low Alkalinity)[#]	1 ½
Top	1/3	1050	58.50	~1.0	1500 (Low Alkalinity)[#]	2

*: "Alamo" type I, white Portland cement, Alamo Cement Co. (San Antonio, TX)

#:"Alamo" type I/II, low alkalinity Portland cement, Alamo Cement Co. (San Antonio, TX)
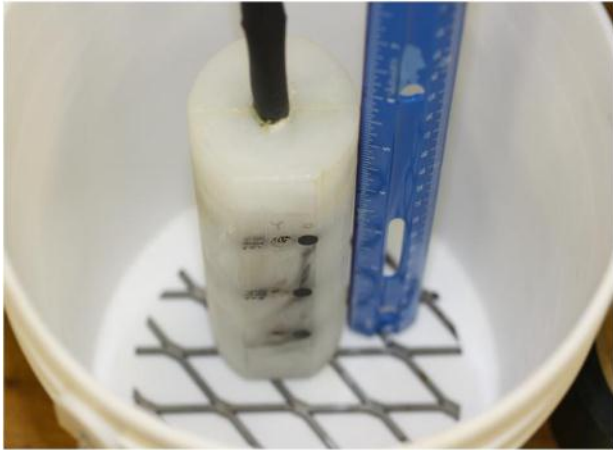
(a)
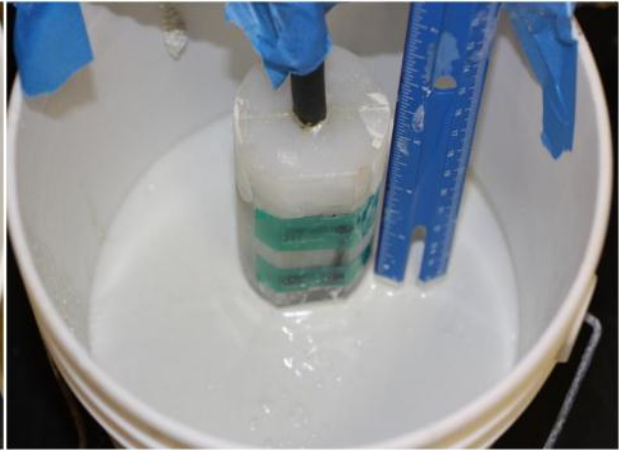
(b)
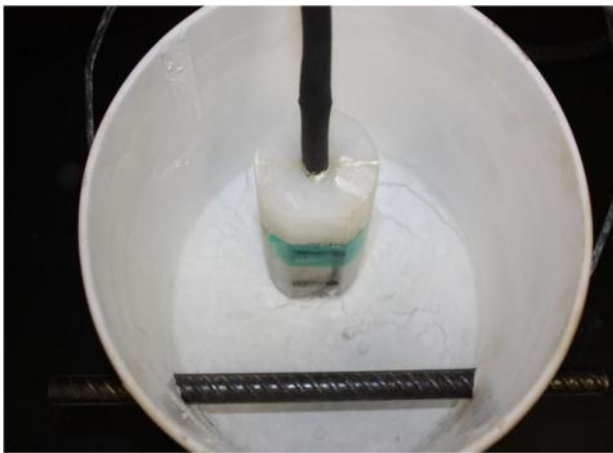
(c)

(d)

(e)

(f)

(g)   (h)

Figure 15. Photographic illustration of the fabrication and curing procedures of paste specimen with multi-probe sensor embedded. (a) Positioning mold and the sensor; (b) Pouring the bottom paste layer(2 ½" thickness); (c) Preparing the middle paste layer after 24 hours of bottom paste layer pouring (with a 6″ length #5 rebar inserted into the mold); (d) Pouring the middle paste layer(1 ½" thickness); (e) Preparing the top paste layer after 24 hours of bottom paste layer pouring (with a 6″ length #5 rebar inserted into the mold); (f) Pouring the top paste layer(2" thickness); (g) de-mold the paste specimen after 24 hours of top paste layer pouring (a small paste cylinder of each layer paste shown was fabricated for further chloride and pH analysis); (h) Placing the specimen in a humidity chamber for 28 days curing process.

The whole specimen was fabricated in three consecutive days. In the first day, the bottom paste layer was poured in 2 ½″ thickness with the bottom sensor set fully immersed (as shown in Figure 15b). The top and middle sensor sets were tape sealed to avoid contamination by the bottom layer paste pouring. Subsequent to pouring, the paste was covered with plastic film and placed in an ambient temperature for 24 hours. On the second day, the plastic film was removed and a well-polished 6″ rebar segment (#5) was inserted into the mold at the same height as the middle probe set (as shown in Figure 15c). Next, the middle layer paste was poured to 1 ½" height submerging the middle sensor set (as shown in Figure 15d) and the inserted rebar segment totally. Similarly, the top sensor set was covered with tape during pouring and the paste was covered with plastic film to avoid water evaporation after pouring. On the third day, after the middle paste layer was cured for 24 hours, the plastic film was removed, a well-polished 6″ rebar segment (#5) was inserted into the mold at the same height as the top probe set (as shown in Figure 15e). The top layer paste was poured to 2" height submerging the top sensor set and the rebar segment totally (as shown in Figure 15f). Subsequently, a plastic film was used to cover the fresh paste for another 24 hours.

Note that a small paste cylinder (1~2" length by 1 ½" diameter) for each individual layer was poured simultaneously for further chloride and pH analysis. Lastly, the paste specimen was removed from the mold as a whole (as shown in Figure 15g). The specimen was placed in a warm humidity chamber to cure for another 28 days. Sensor lead wires were connected

to the board and the corrosion rates of MAS probes and the potential readings of chloride probes were collected during the curing process.

After 28 days of curing, the paste specimen was removed from the wet curing chamber and placed in a 50°C dry oven for another 30 days. This procedure was performed to evaporate the moisture inside the specimen. Subsequently, the specimen was removed from the oven. Several micro-cracks were visually observed on top of the specimen, likely caused by drying shrinkage. The drying and cracking were designed to accelerate the ingress of external chloride into the paste specimen, thus reducing the time required for observing significant changes in the sensor readings.

Then, a 6″ diameter by 4″ length of a plastic tube section was glued on to the top of the specimen as a ponding reservoir. Once the glue is cured, 500 mL 3.5% NaCl solution was poured into the pond. The pond was covered with a plastic lid to minimize evaporation of the NaCl solution. Two days later, the NaCl solution was totally sucked into the specimen through capillary water absorption. Ponding 500 mL 3.5% solution into the reservoir was repeated three times. It took about 7 days for the solution to be totally "sucked" into the specimen for the third ponding, indicating that the rate of water absorption dropped significantly as the paste became nearly water-saturated. In addition, there was water percolation at the bottom of specimen in the 3rd NaCl ponding duration, again confirming the water saturation of the specimen.

To further accelerate the chloride ingress into the specimen, an external electric field was applied to the paste specimen. Note that, throughout the implementation of the electric field, the specimen was placed in a 1″ deep bath of saturated $Ca(OH)_2$ with a 2″ depth of 3.5% NaCl solution in the pond reservoir. The bath is to increase the electrical conductivity of the bottom part of the specimen. A piece of stainless steel (SS) mesh (5″ length by 4″ width) was placed at the bottom of the ponding reservoir (as shown in Figure 16a) as an auxiliary electrode. As shown in Figure 16b, this SS mesh and the SS mesh embedded at the bottom of the specimen were wire connected to a DC power supplier to provide the current required for chloride ingress into the specimen from the top to the bottom. A constant current (0.1mA) was applied through the SS meshes for three days. Subsequently, the current was stepped up and held at 0.2, 0.5, 1.0 mA for 3 or 4 days in each step. The LPR of the two embedded rebar was measured periodically at the end of each current step. The results were used to validate the variation of corrosion rate readings of MAS probes and the chloride concentration calculated from readings of the chloride probe.

(a)

(b)

Figure 16. Photographic illustration of the benchmark test at SwRI: (a) ponding reservoir; (b) setup for electrical injection of chloride into the specimen (0.5A DC current applied).

Figure 17 shows the temporal evolution of corrosion rates, including general and max localized corrosion, as function as exposure time. The test was started on June 29, 2012, the beginning of the curing process for the specimen, and ended on November 20, 2012. Data were lost from 10/15/2012 to 10/30/2012 as the battery for the MAS board died. The service life of the battery in this test was limited because the data acquisition frequency was 15 minutes in the first three and a half months. The same battery for the board was used previously for the benchmark test with the same 15-minute data acquisition frequency for approximately two months. For field implementation, the data acquisition frequency is set at every 6 hours; as such, we anticipate the battery life of more than three years.

During the test, some issue occurred to the firmware embedded in the MAS board. The issue made the total of 16 pins counted as one MAS probe and the indicated general corrosion and maximum localized corrosion rates representing the average and maximum values of the 16 pins. According to the sensor prototype, the data should be separated into two groups. The data collected from pin 1~8 should represent the results of MAS probe in the top (near the cable) probe set and data collected from pin 9~16 should represent the results of MAS probe in the middle probe set. The comparison of the two groups of data should project corrosion status of rebars at different depths. The firmware has been adjusted afterwards and the issue has been resolved.
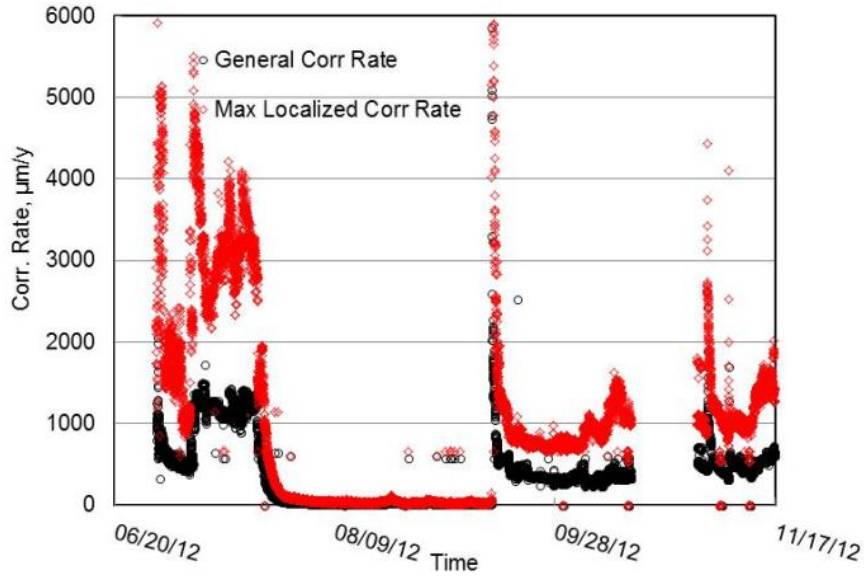
(a)
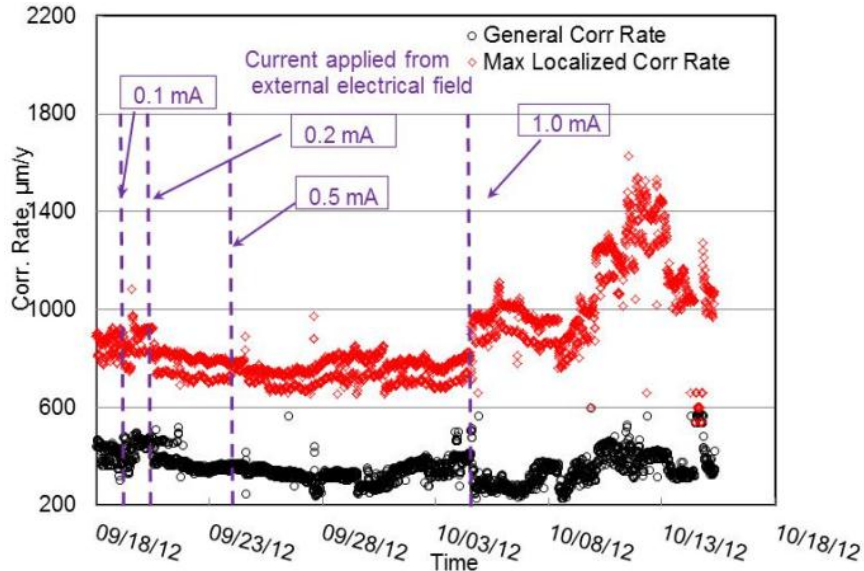
(b)

Figure 17. Temporal evolution of corrosion rates, including general and maximum localized corrosion rates, as a function of exposure time

Regardless the issues of the firmware, the results of general and maximum localized corrosion rates indicated as one MAS probe still offer valuable information about the sensor. During the curing process (6/28/2012 to 7/25/2012), the MAS probe experienced severe corrosion attack. As shown in Figure 17a, the general corrosion rates stabilized in the range of 700 and 1200 µm/y and the max localized corrosion rates fluctuate between 1000 and 6000 µm/y. The high corrosion rates are reasonable since: (1) significant amount of chloride was mixed in the paste and a protective passive film could not form on the MAS pin surfaces; (2) the warm (~50°C) and wet (90% humidity) environment facilitated the conductive path between pins and facilitated the corrosion propagation.

35

After curing, the paste specimen was placed at the SwRI laboratory with a dry and ambient temperature from 7/25/2012 to 9/13/2012. As the moisture inside the paste specimen evaporated, the MAS probe exhibited very low corrosion rates (as shown in Figure 17a).

Figure 17b illustrates the effect of applying external electric field on the MAS probe readings, with the data from 9/19/2012 to 11/20/2012 plotted in the expanded format. The data reveal that only when the applied electric field reached 1.0 mA/cm^2 significant increase in the MAS corrosion rates were observed.

Figure 18 shows the temporal evolution of SwRI chloride probe potentials and pH probe readings, as function as exposure time. The bottom Cl probe showed unusually positive potential readings (in contrast to the typically negative readings seen in Figure 11), suggesting its possible malfunctioning. As significant amount of external chloride was injected by the electric field (from 9/19/2012 to 11/20/2012), the Cl probes at the middle and top locations showed significantly difference in their potential readings. The middle Cl probe typically exhibited more positive potentials, corresponding to lower chloride concentration at its surface (this is consistent with Figure 20 in a later section), relative to the top Cl probe. This indirectly validates the performance of these two Cl probes. Data from 10/15/2012 to 10/30/2012 were erroneous as the battery for the MAS board died.

As shown in Figure 18b, the bottom pH probe showed unusually low pH readings, which combined with Figure 18a suggest a likely failure of the bottom graphite reference electrode. The early-age readings of both top and middle pH probes fluctuated between pH 8 and 10, suggesting likely carbonation of the paste. As significant amount of hydroxyls was produced near the SS mesh in the pond (cathode) by the electric field (from 9/19/2012 to 11/20/2012), the top probe detected significantly higher pH values than the middle probe, indirectly validating the performance of these two probes. Again, data from 10/15/2012 to 10/30/2012 were erroneous as the battery for the MAS board died.

While more research is needed, the data field from 9/19/2012 to 11/20/2012 also imply that the MAS probes (Figure 17b), Cl probes (Figure 18a) and pH probes (Figure 18b) all have great potential to work properly under a reasonably low electric field. If they are strategically placed in the concrete, these probes could potentially be used in conjunction with impressed current cathodic protection (ICCP) to automatically adjust the protective current in a way that maximizes anode life and optimizes corrosion control.
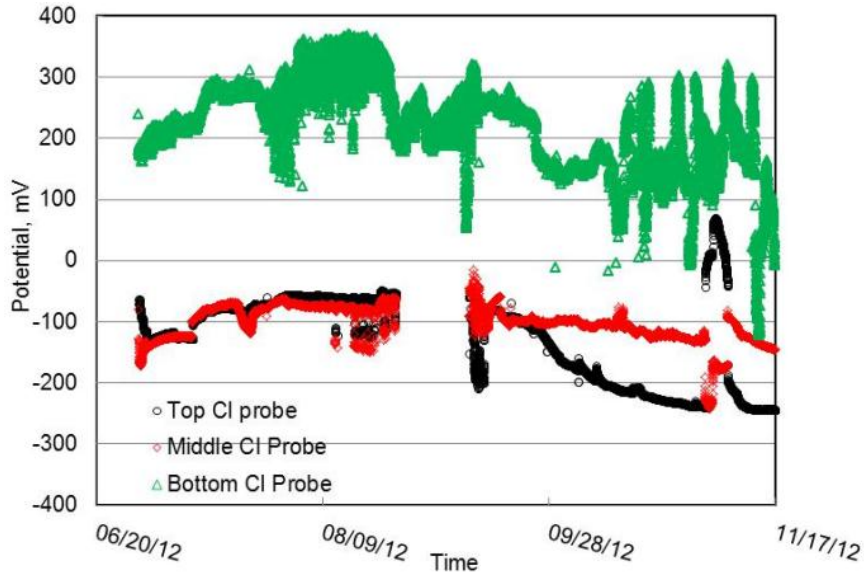
(a)
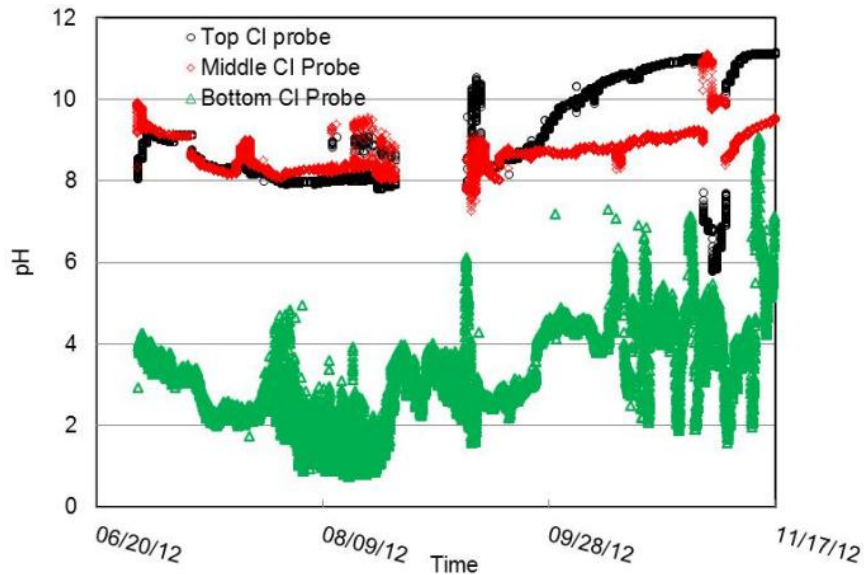
(b)

Figure 18. Temporal evolution of (a) Ag/AgCl probe potentials and (b) pH in paste as a function of exposure time

2.4. Accelerated Testing of Sensor Longevity

At the WTI CSIL, the custom-made chloride probes along with the SwRI sensor (as shown in Figure 4), a conventional Ag/AgCl probe (as control), and three rust-free, bare steel #4 rebars (immersed length: 2″) went through a cyclic immersion in the simulated concrete pore solutions. Each sensor went through an immersion cycle for a period of two weeks and drying cycle for 3 days. During each wetting cycle, the potential difference of each sensor was measured against SCE for every hour using the data acquisition system. The

potentiometric response of each sensor was also measured against SCE before and after each immersion cycle to measure linearity.

As shown in Table 2, only six out of the eighteen WTI custom-made chloride probes (WTI Cl1a, WTI Cl1b, WTI Cl2a, WTI Cl2b, WTI Cl1c, and WTI Cl3) can be considered reliable after the eight cycles of weathering (consisting of wet-dry and chloride concentration changes). The coefficients of variance (COVs) highlighted in red color indicate values higher than 20%, which was used as a cut-off value for identifying poor sensor stability in the test solution with a given chloride concentration. In other words, the ideal probe would feature a very stable potential reading during each cycle, which would translate to a COV value of approximately 0%.

As shown in Table 3, the control Cl⁻ probe (Ag/AgCl via electrodeposition only) failed to remain reliable after cycle 4, likely due to the degradation of AgCl surface layer by the alkaline oxidation and wet-dry cycling. Two of three SwRI chloride probes remained reliable after the eight weathering cycles, whereas the 2nd SwRI chloride probe failed to remain reliable after cycle 6. All three SwRI graphite probes remained reliable after the eight weathering cycles. Note that after cycle 4 (Cl⁻ increased from 0.03M to 0.04M), the 3rd rebar exhibited great variability in its potential readings during each cycle, which is attributable to its active corrosion.

Table 2. Potentiometric responses of WTI custom-made Ag/AgCl probes during the weathering cycles

Name of the chloride sensor	Cycle 1			Cycle 2			Cycle 3			Cycle 4			Cycle 5			Cycle 6			Cycle 7			Cycle 8		
	Average	STDEV	COV	Average	STDEV	COV	Average	STDEV	COV	Average	STDEV	COV	Average	STDEV	COV	Average	STDEV	COV	Average	STDEV	COV	Average	STDEV	COV
Amberlite IRA - 400 Chloride	-722.4	323.9	-45%	-323.7	29.1	-9%	-378.9	51.1	-13%	-569.8	225.8	-40%	-896.1	129.5	-14%	-1001.2	239.3	-24%	-1033.1	79.0	-8%	-895.9	52.4	-6%
Polyethylene Oxide	-310.1	18.4	-6%	-328.1	17.8	-5%	-331.9	37.0	-11%	-342.1	30.1	-9%	-365.2	113.4	-31%	-356.5	36.9	-10%	-314.3	56.0	-18%	-376.7	70.4	-19%
WTI Cl1a	-159.2	8.0	-5%	-170.0	6.3	-4%	-156.7	13.3	-8%	-155.5	9.3	-6%	-170.0	5.6	-3%	-171.1	10.5	-6%	-157.3	7.2	-5%	-178.3	6.7	-4%
Polytetrafluroethylene	-416.1	70.5	-17%	-409.1	99.8	-24%	-411.7	76.9	-19%	-484.4	163.8	-34%	-973.2	118.3	-12%	-951.1	59.3	-6%	-876.2	81.8	-9%	-914.7	103.4	-11%
Poly Vinyl alcohol	-721.8	305.3	-42%	-763.0	334.3	-44%	-679.8	283.1	-42%	-649.7	303.7	-47%	-934.3	275.5	-29%									
Dextrose (Glucose) Anhyrdous	-378.4	40.9	-11%	-426.7	156.4	-37%	-499.2	217.4	-44%	-454.7	190.4	-42%	-924.6	95.3	-10%									
WTI Cl1b	-158.1	9.4	-6%	-172.4	9.2	-5%	-171.2	5.7	-3%	-167.9	7.0	-4%	-185.8	5.9	-3%	-207.6	9.7	-5%	-220.4	18.0	-8%	-252.7	12.6	-5%
Chitosan	-368.1	24.8	-7%	-820.9	322.6	-39%	-1068.7	99.4	-9%	-1055.8	97.2	-9%	-1111.2	61.9	-6%	-984.9	128.8	-13%	-774.7	43.9	-6%	-925.5	118.0	-13%
WTI Cl2a	-163.1	9.2	-6%	-174.4	11.0	-6%	-180.5	4.6	-3%	-181.0	10.4	-6%	-216.9	10.9	-5%	-252.3	15.9	-6%	-271.9	33.5	-12%	-321.8	29.7	-9%
Chitosan	-352.4	18.0	-5%	-370.2	36.3	-10%	-400.6	97.7	-24%	-360.6	57.7	-16%	-567.0	291.8	-51%	-1001.7	101.4	-10%	-709.3	203.5	-29%	-861.9	127.4	-15%
Polyethylene Glycol	-305.2	15.3	-5%	-343.1	46.9	-14%	-412.7	102.8	-25%	-342.2	116.6	-34%	-874.2	183.0	-21%	-737.1	236.6	-32%	-832.3	172.1	-21%	-890.0	94.7	-11%
Chitosan	-1047.4	140.4	-13%	-1067.6	70.8	-7%	-988.6	129.3	-13%	-815.8	230.2	-28%	-992.9	127.9	-13%	-867.6	93.9	-11%	-893.0	121.9	-14%	-907.0	96.4	-11%
poly Vinyl Alcohol	-344.9	30.3	-9%	-369.6	61.7	-17%	-477.7	193.5	-41%	-511.9	226.5	-44%	-1022.8	121.8	-12%									
Poly Acrylic acid	-354.4	21.5	-6%	-399.8	56.5	-14%	-467.4	132.6	-28%	-502.3	219.4	-44%	-1094.1	131.9	-12%									
Poly Vinyl Alcohol	-1036.8	157.8	-15%	-896.9	233.6	-26%	-934.8	136.2	-15%	-979.4	82.3	-8%	-1041.5	89.2	-9%	-775.0	12.7	-2%	-916.2	126.3	-14%	-1077.2	58.8	-5%
WTI Cl2b	-167.2	13.5	-8%	-179.3	7.5	-4%	-174.3	8.2	-5%	-172.0	7.2	-4%	-197.3	6.6	-3%	-220.2	9.1	-4%	-216.9	9.6	-4%	-241.9	8.3	-3%
WTI Cl1c	-266.4	13.1	-5%	-266.1	14.2	-5%	-281.9	17.3	-6%	-269.3	15.5	-6%	-287.2	16.2	-6%	-304.7	23.8	-8%	-276.9	23.9	-9%	-303.5	8.5	-3%
WTI Cl3	-330.2	30.9	-9%	-374.3	37.3	-10%	-358.8	26.3	-7%	-341.5	20.1	-6%	-370.9	26.4	-7%	-367.0	22.3	-6%	-348.2	19.7	-6%	-406.4	51.7	-13%

* The grey color indicates sensors being removed from the test due to poor linearity measured in proceeding cycles.
Note: The potential of chloride probes was measured against a SCE.

Table 3. Potentiometric responses of the SwRI sensing probes (and the control Cl⁻ probe) during the weathering cycles

Sensors	Cycle 1			Cycle 2			Cycle 3			Cycle 4			Cycle 5			Cycle 6			Cycle 7			Cycle 8		
	Average	STDEV	COV	Average	STDEV	COV	Average	STDEV	COV	Average	STDEV	COV	Average	STDEV	COV	Average	STDEV	COV	Average	STDEV	COV	Average	STDEV	COV
REBAR(1)	-161.9	18.0	-11%	-136.6	7.3	-5%	-151.9	20.3	-13%	-115.1	8.8	-8%	-118.7	7.0	-6%	-125.1	10.8	-9%	-107.9	33.3	-31%	-121.1	31.4	-26%
REBAR(2)	-155.9	10.7	-7%	-141.9	10.9	-8%	-134.9	2.4	-2%	-166.6	58.7	-35%	-131.3	26.3	-20%	-123.3	10.0	-8%	-100.0	9.7	-10%	-124.6	8.5	-7%
REBAR(3)	-184.0	42.9	-23%	-159.4	39.9	-25%	-124.1	20.7	-17%	-161.9	31.0	-19%	-116.4	767.6	-660%	-142.9	105.7	-74%	-324.9	66.7	-21%	-159.6	852.4	-534%
Control Cl	-203.8	13.1	-6%	-202.3	17.4	-9%	-188.0	16.2	-9%	-278.3	47.5	-17%	-495.8	244.7	-49%	-526.5	296.3	-56%	-297.9	40.5	-14%	-478.4	212.6	-44%
SWRI_CL(1)	282.7	3.5	1%	283.8	4.6	2%	261.0	18.5	7%	261.9	3.2	1%	259.7	5.8	2%	235.5	5.1	2%	206.2	23.1	11%	224.5	19.3	9%
SWRI_CL(2)	271.5	11.2	4%	275.4	28.8	10%	245.7	26.8	11%	227.1	31.3	14%	217.6	35.0	16%	145.7	47.7	33%	146.9	73.7	50%	126.3	49.0	39%
SWRI_CL(3)	267.1	9.1	3%	269.6	16.3	6%	261.4	14.1	5%	272.0	15.9	6%	297.6	18.3	6%	306.2	28.9	9%	335.1	38.2	11%	311.3	44.0	14%
GTE_SCE(1)	-186.5	3.2	-2%	-183.2	8.6	-5%	-156.5	21.5	-14%	-167.8	9.3	-6%	-174.3	6.2	-4%	-179.0	4.4	-2%	-164.8	12.6	-8%	-187.3	8.2	-4%
GTE_SCE(2)	-177.1	10.4	-6%	-193.3	14.0	-7%	-180.9	14.7	-8%	-194.1	16.3	-8%	-243.9	9.1	-4%	-256.5	4.0	-2%	-212.1	17.6	-8%	-244.1	4.8	-2%
GTE_SCE(3)	-174.8	4.5	-3%	-180.9	14.7	-8%	-173.8	18.7	-11%	-199.5	14.9	-7%	-228.2	10.5	-5%	-267.4	17.3	-6%	-293.2	40.5	-14%	-274.9	41.2	-15%

Note: The potential of control chloride probe, rebars, and graphite probes was measured against a SCE, whereas that of the SwRI chloride probes was measured against their closest graphite probe.

It should be noted that the temperature in existing concrete structures would rarely (if ever) reach as high as 104ºF and the use of this relatively high temperature aims to accelerate the possible oxidation and degradation of the sensing elements once they are embedded in concrete. Similarly, the sensing elements in field concrete would rarely be completely dry. The alternated wetting and drying aim to capture the effects of moisture fluctuations experienced by the field concrete on the stability of the embedded sensing elements.

The accelerated laboratory testing results should indicate whether the critical sensing elements can retain their sensing properties and integrity after being subjected to aggressive service environments. The results will also provide preliminary information regarding sensor life in field applications.

During the testing of sensor longevity, instead of periodically measuring the anodic current flowing between the MAS pins (i.e, ΔI_{ij}), we periodically measured the potential difference between the MAS pins ((i.e, ΔE_{ic}, with the central pin as reference). The potential difference between certain MAS pins (e.g., ΔE_{ij}) was not directly measured but was calculated using the following equation:

$$\Delta E_{ij} = \Delta E_{ic} - \Delta E_{jc}$$

All the ΔE values were taken at their absolute values and subsequently the maximum and average ΔE of each MAS probe in a given test solution was monitored on an hourly basis during the weathering cycles (except the drying periods). Note that one of the MAS probe featured 9 identical small pins whereas the other MAS probe featured 3 small pins and 3 large pins due to short-circuiting.

As shown in Figure 19a, for the 9-pin MAS, the following three parameters showed strong correlation with the chloride concentration of the simulated pore solutions: (1) *maximum of maximum ΔE*, (2) *maximum of average ΔE*, and (3) *average of average ΔE / average of maximum ΔE*. The first two parameters peaked in the range of 0.04 to 0.06 M chloride concentration, whereas the 3rd parameter decreased and the rebar potential increased as the chloride concentration increased. These trends coincide with the trends observed in the corrosion rates measured by MAS and by rebar respectively, as illustrated earlier in Figure 14.

As shown in Figure 19b, for the 6-pin MAS, the following three parameters showed strong correlation with the chloride concentration of the simulated pore solutions: (1) *average of maximum ΔE*, (2) *average of average ΔE*, and (3) *average of average ΔE / maximum of maximum ΔE*. The first two parameters peaked in the range of 0.04 to 0.06 M chloride concentration, whereas the 3rd parameter decreased and the rebar potential increased as the chloride concentration increased. These trends coincide with the trends observed in the corrosion rates measured by MAS and by rebar respectively, as illustrated earlier in Figure 14. *The 3rd parameter may hold the promise of using 6-pin MAS as a very good tool to predict the rebar corrosion rate even in the case of active corrosion and high chloride concentration, which warrant additional research.*

41
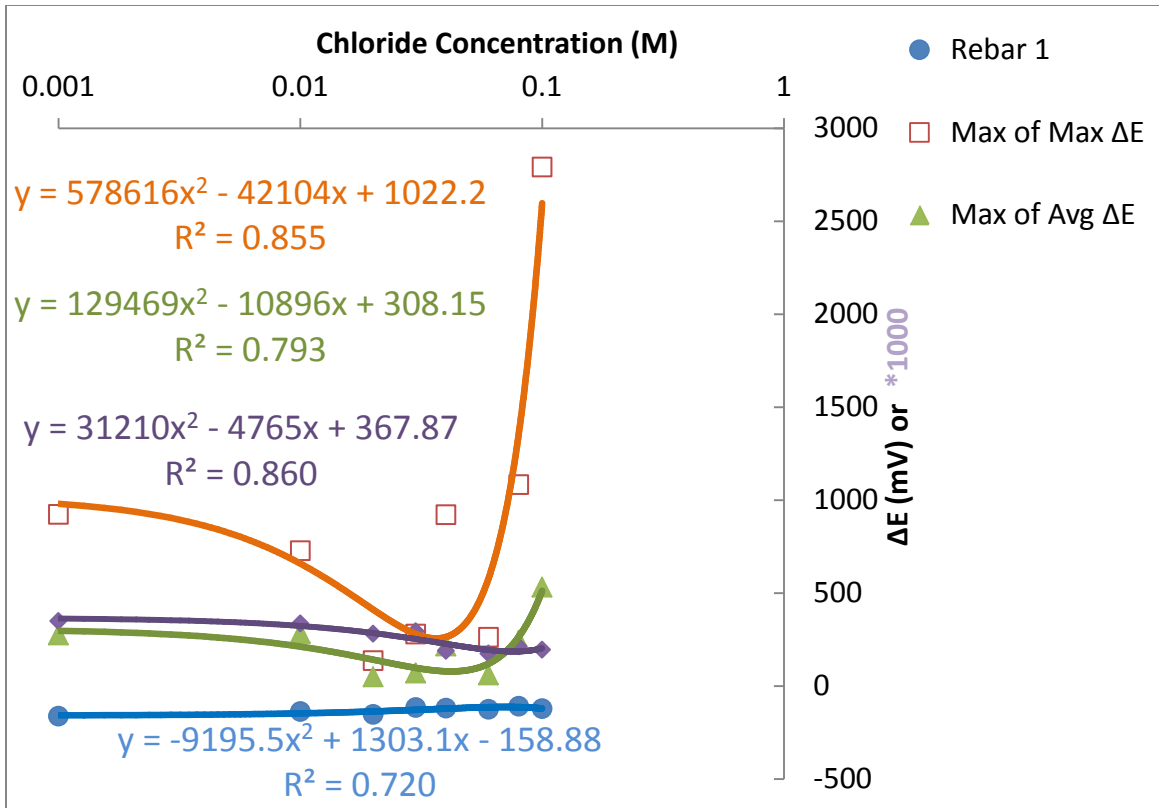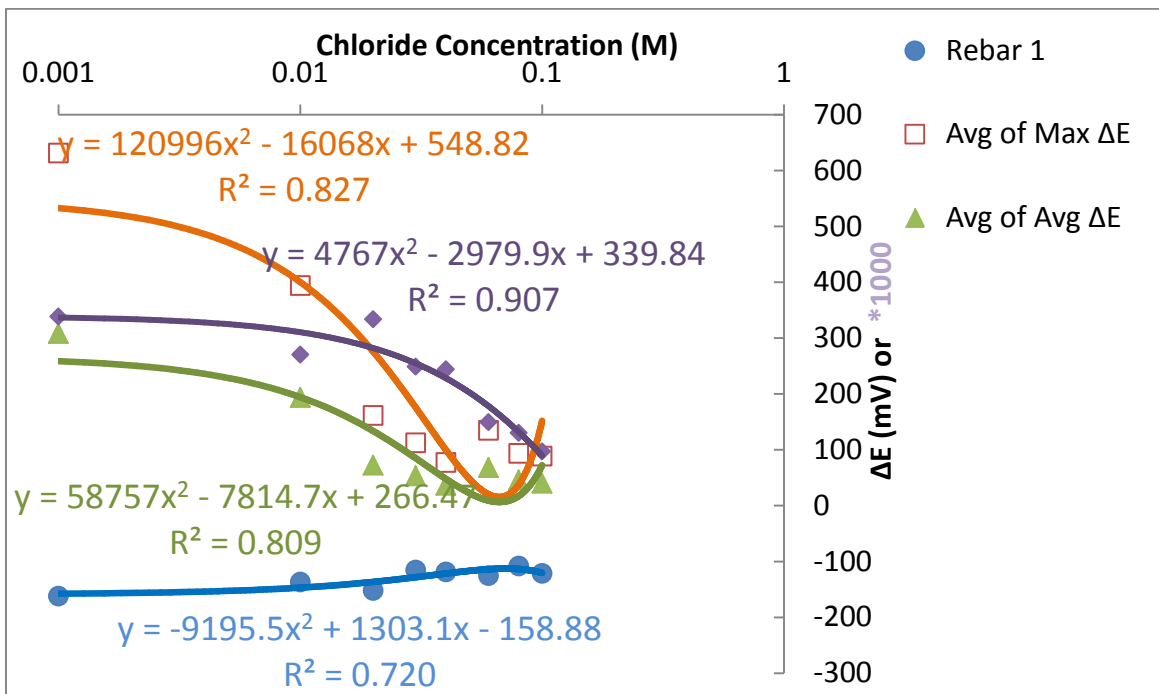
Figure 19. MAS and rebar data as a function of chloride concentration of simulated pore solutions over the eight weathering cycles: (a) MAS with 9 identical pins; (b) MAS with 6 different pins

As shown in Figure 20, only three out of the eighteen WTI custom-made chloride probes (WTI Cl1b, WTI Cl2a, and WTI Cl3) can be considered reliable chloride probes after the eight cycles of weathering. This is based on the fact that their average potential reading maintained a high 2nd-order polynomial correlation (0.88 or above) with the chloride concentration of simulated pore solution, over the eight weathering cycles. In contrast, two of the three SwRI Ag/AgCl probes (SwRI Cl2 and SwRI Cl1) may be considered reliable chloride probes after the eight cycles of weathering, whereas the SwRI Cl3 probe exhibited a relatively weaker correlation (R-square of 0.795). Note that as the chloride concentration increased, the Cl probe potential generally decreased (except for SwRI Cl3). This contradicts the trend observed in the benchmark test (see Figure 11) but is consistent with the theory of electrochemical equilibrium (Nernst Equation).

As discussed earlier (As shown in TABLE 3), the 2nd SwRI chloride probe failed to remain reliable after cycle 6 and showed high COV values during cycles 7 and 8. In other words, *only one of the three SwRI Ag/AgCl probes can be considered reliable chloride probes. This highlight the need for further improving the approach to fabricate the Ag/AgCl probes to serve as chloride probes in concrete. Meanwhile, the three WTI custom-made chloride probes (with the appropriate treatment by proprietary coating) showed great promise in this regard.*

Finally, as shown in Figure 20, the control Cl⁻ probe (Ag/AgCl via electrodeposition only) failed to exhibit a good correlation between its average potential reading with the chloride concentration of simulated pore solution, over the eight weathering cycles. The R-square in this case was only 0.562, indirectly confirming the superior longevity of custom-made SwRI and WTI chloride probes.
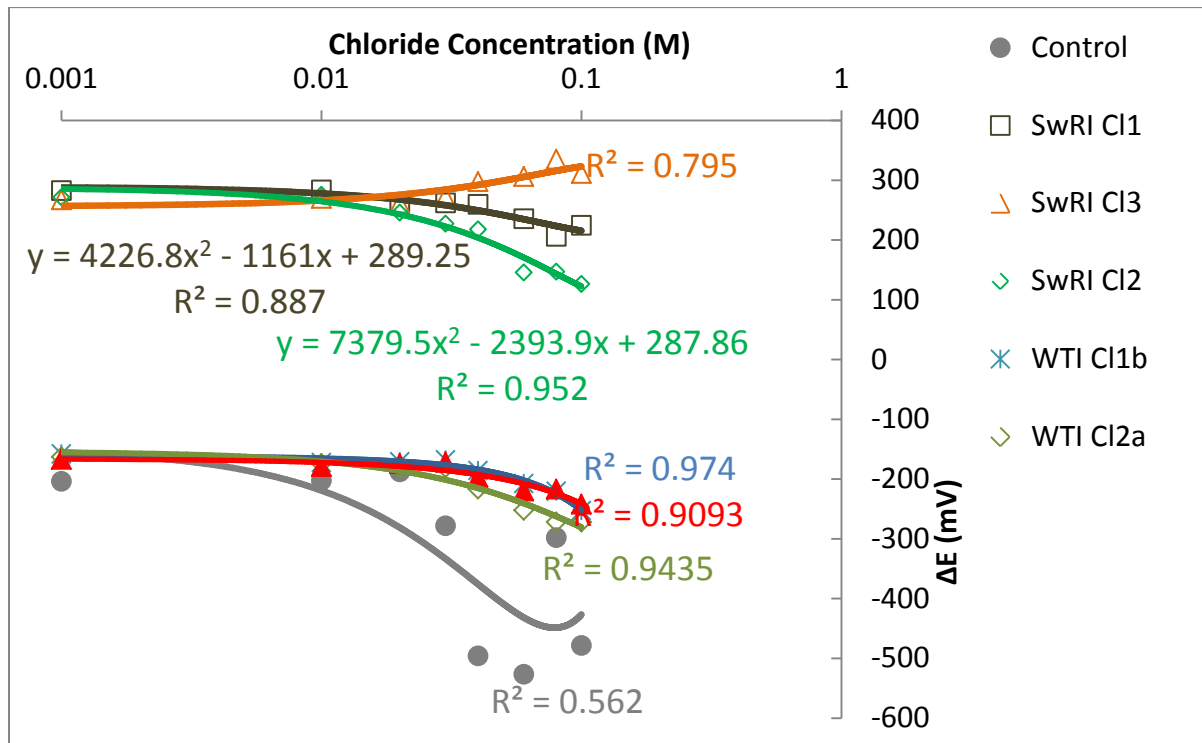
Figure 20. WTI and SwRI chloride probes as a function of chloride concentration of simulated pore solutions over the eight weathering cycles

Note that the potential of control chloride probe and WTI chloride probes was measured against a SCE, whereas that of the SwRI chloride probes was measured against their closest graphite probe. As shown in TABLE 4, this may have partially contributed to the high variability observed in the measurements by the SwRI chloride probes. Table 4 reveals that *over the eight weathering cycles, only one of the SwRI graphite probes (GTE_SCE(1)) remained relatively stable, with its potential showing a standard deviation of 11 mV and a COV of -6%. Interestingly, a few of the WTI custom-made Ag/AgCl probes (WTI Cl1a and WTI Cl1c) showed good potential to serve as reliable reference electrodes in concrete.*

Table 4. Potentiometric responses of the SwRI reference probes and WTI reference probes during the weathering cycles

Cycle	Solution (Cl⁻, M)	WTI Cl1a	WTI Cl2b	WTI Cl1c	WTI Cl3	GTE_SCE(1)	GTE_SCE(2)	GTE_SCE(3)
1	0.001	-159.2	-167.2	-266.4	-330.2	-186.5	-177.1	-174.8
2	0.01	-170.0	-179.3	-266.1	-374.3	-183.2	-193.3	-180.9
3	0.02	-156.7	-174.3	-281.9	-358.8	-156.5	-180.9	-173.8
4	0.03	-155.5	-172.0	-269.3	-341.5	-167.8	-194.1	-199.5
5	0.04	-170.0	-197.3	-287.2	-370.9	-174.3	-243.9	-228.2
6	0.06	-171.1	-220.2	-304.7	-367.0	-179.0	-256.5	-267.4
7	0.08	-157.3	-216.9	-276.9	-348.2	-164.8	-212.1	-293.2
8	0.1	-178.3	-241.9	-303.5	-406.4	-187.3	-244.1	-274.9
	COV	-5%	-14%	-6%	-6%	-6%	-15%	-22%
	Average	-165	-196	-282	-362	-175	-213	-224
	Standard Dev.	9	27	16	23	11	31	49

Table 5 shows the variability of potential readings of various sensing probes within 60 s of immersion into a simulated pore solution with 0.03M NaCl, with readings taken every 10 s. This sheds light on the response time of the sensing probes. The vast majority of WTI custom-made Ag/AgCl probes (except WTI Cl1b) exhibited rapid response time as their potential quickly stabilized in the test solution. In comparison, the SwRI sensing probes featured a slightly higher variability in their 60-s potential readings, indicating a slightly longer response time. Nonetheless, we can conclude that *the vast majority of the sensing probes featured a response time of less than 60 seconds.*

Table 5. Response time of various sensing probes, measured by the potential variability within 60 s of immersion into a simulated pore solution with 0.03 M NaCl.

Name of the WTI Cl sensor	Average	Stdev	COV	Name of the SwRI sensor	Average	Stdev	COV
Amberlite IRA - 400 Chloride	-826.8	0.4	-0.05%	Surafce sensor 1 -1	-61.5	0.9	-1.5%
Polyethylene Oxide	-266.5	0.2	-0.09%	Surafce sensor 1 -2	-59.7	0.5	-0.9%
WTI Cl1a	-123.7	0.3	-0.22%	Surafce sensor 1 -3	-57.7	0.7	-1.3%
Polytetrafluroethylene	-821.8	0.4	-0.05%	Surafce sensor 1 -4	-55.7	0.6	-1.0%
Poly Vinyl alcohol				Surafce sensor 1 -5	-54.0	0.7	-1.2%
Dextrose (Glucose) Anhyrdous				Surafce sensor 1 -6	-52.1	0.7	-1.3%
WTI Cl1b	-19.3	16.2	-83.88%	Surafce sensor 1 -7	-50.4	0.7	-1.3%
Chitosan	-97.6	0.9	-0.90%	Surafce sensor 1 -8	-48.8	0.7	-1.4%
WTI Cl2a	-95.0	0.7	-0.72%				
Chitosan	-92.0	0.7	-0.77%	Surafce sensor 2 -1	-47.2	0.7	-1.6%
Polyethylene Glycol	-89.3	0.7	-0.78%	Surafce sensor 2 -2	-45.6	0.6	-1.3%
Chitosan	-86.8	0.6	-0.70%	Surafce sensor 2 -3	-43.9	0.7	-1.5%
poly Vinyl Alcohol				Surafce sensor 2 -4	-42.4	0.9	-2.1%
Poly Acrylic acid				Surafce sensor 2 -5	-40.9	0.8	-2.1%
Poly Vinyl Alcohol	-78.9	0.8	-1.03%	SWRI - 1	-39.5	0.9	-2.3%
WTI Cl2b	-76.8	1.0	-1.27%	SWRI - 2	-38.0	0.8	-2.0%
WTI Cl1c	-74.5	0.6	-0.76%	SWRI - 3	-36.7	0.8	-2.2%
WTI Cl3	-72.0	0.6	-0.82%	Control Cl sensor	-63.7	0.5	-0.8%

2.5. Methodology for Sensor Data QC and Interpretation

2.5.1 Algorithm for the Prediction of Remaining Service Life

Reinforcement corrosion induced by chloride contamination is a leading cause of structural damage and premature degradation in RC structures. It is critical to monitor the health status of structures to ensure safety of traffic and transportation infrastructures. The appearance of the first corrosion crack is usually used to define the end of functional service life, under which rehabilitation of associated structures is required [1-2]. Hence, a key element in the evaluation of service life is to predict corrosion cracking [3].

In the study by Tuutti [1], there are two phases in deterioration caused by corrosion: the initiation phase and the propagation phase. The initiation phase is the time required for sufficient CO_2 and Cl^- ions to reach the steel-concrete interface and activate corrosion. The propagation phase is the time between corrosion initiation and corrosion cracking, in which the accelerated corrosion of the RC structure ultimately leads to cracking. Weyers [2] further divide the propagation phase into two different periods, the free expansion period and the stress build-up period. Under the propagation phase, a more reactive maintenance strategy would be necessary. Therefore, the prediction of time-to-corrosion-initiation due to ingress of Cl^- ions is crucial.

According to the Fick's Second law, chloride ion migration into water-saturated concrete is an ionic diffusion process. Fick's second law represents non-steady state diffusion and is shown by the following partial differential equation:

$$\frac{\partial C}{\partial t} = \frac{\partial}{\partial x}\left(D\frac{\partial C}{\partial x}\right)$$

(1)

where C = chloride ion concentration
D = diffusion coefficient
t = time
x = depth

Depending on the boundary conditions, the above equation has many solutions. The most common solutions use the boundary conditions of $C(x=0)=C_s$ (constant chloride surface concentration) and C_0 (original chloride concentration in concrete as a constant). Usually C_0 is set as 0. Then Fick's second law becomes:

$$C(x,t)=C_0+(C_S-C_0)\left[1-\mathrm{erf}\left(\frac{x}{2\sqrt{Dt}}\right)\right]$$

(2)

where C(x,t) = chloride concentration at depth x after time t
D = diffusion coefficient
erf = error function

Assuming one-directional diffusion of chloride, the diffusion coefficient can be obtained by using the chloride probes placed at three different depths (Cl$_1$, X$_1$,), (Cl$_2$, X$_2$), (Cl$_3$, X$_3$) as well as the surface chloride concentration (C$_s$, 0). To calculate the time to corrosion initiation, a critical value of chloride concentration at the rebar depth is used, that is, Cl$_{th}$/[OH$^-$] = constant . A constant value of 1.4 is assumed in this study, based on existing literature. Then, Equation 2 becomes:

$$C_{th} = C_0 + \left(C_s - C_0\right)\left[1-erf\left(\frac{X_r}{2\sqrt{DT_{th}}}\right)\right]$$

(3)

where   X$_r$ = rebar depth

Based on Equation 3, the time of corrosion initiation T$_{th}$ can be obtained. The remaining service life of the RC structure is then calculated by:

T = (T$_{th}$ – t) + T$_{add}$

(4)

where T$_{th}$ – t = the time period to corrosion initiation

T_{add} = a constant value (e.g., 3 years in this case, assumed for the time needed for corrosion propagation to concrete cracking).

2.5.2. Qualify Control of Sensor Data

Observational data are subject to systematic and random errors. The quality control (QC) of sensor data is an essential first step before using the data for predicting the remaining service life of the RC structure. In this study, corrosion rate, chloride, pH, and temperature sensors are deployed to provide measurements for prediction. QC schemes should be developed to make sure that data used for the calculations are with acceptable accuracy. Three types of sensors status are used based on data quality control: normal, questionable, and malfunctioning.

For the corrosion rate sensor, the following rules are developed:

- If the corrosion rate value (CR_n) is negative, then the status is malfunctioning.
- If the current corrosion rate value is less than the value measured during last time interval, then the status is questionable
- a) If the corrosion rate jumped from a value smaller than 0.1 µA/cm^2 (measured at the last time interval) to one greater than 1.0 µA/cm^2 (measured at current time interval), then the status is questionable.
  b) Predict the corrosion rate value (CR_n') based on the values developed in the previous time intervals (1,2,…, n-1), by using polynomial regression. If $|(CR_n' - CR_n)/ CR_n'| > 0.2$, then sensor status is questionable.
- Otherwise, the status is normal. Under normal status, the status of corrosion is "passive" if the corrosion rate value is less than 0.1 µA/cm^2; "transitional" if the value falls between 0.1 and 1.0 µA/cm^2; and "active corrosion" if greater than 1.0 µA/cm^2.

For the temperature sensor, if the reading is out of the range of (-35°F, 105°F), then the sensor status is questionable. If no readings available, the sensor is malfunctioning.

For the pH sensor, if the reading is out of the range of (8, 13.8), then the sensor status is questionable. If no readings available, the sensor is malfunctioning.

For chloride probes, a two-phase quality control scheme is developed.

Phase 1:
1) At time interval n (or time t_n), assume all three sensors are working normally.
2) If the chloride concentration for a given sensor is negative (or null value), then the status is malfunctioning.
3) If the chloride concentration for a given sensor is greater than 2.0 M, then the status is questionable.
4) If at least two sensors are marked as normal, apply the data to Equation 2 to obtain the diffusion coefficient (D_n) at time interval n. Predict the diffusion coefficient value (D_n') based on the diffusion coefficient values developed in the previous time intervals (1,2,…, n-1), by using polynomial regression. If $|(D_n' - D_n)/ D_n'| < 0.2$, then finish data quality control. Otherwise, continue to Phase 2.

Phase 2:

1) If three chloride and corrosion rate sensors are all normal, use the following table to calculate service life.

	$CR_n < 0.1$	$0.1 < CR_n < 1$	$CR_n > 1$
$T_{th(n)} > t_n$	$T_n = T_{th(n)} - t_n + T_{add}$	$T_n = T_{th(n)} - t_n + T_{add}$	If $T_{n-1} > t$, $T_s = T_{th} - t + T_{add}$ Otherwise, $T_n = T_{add}$ (Chloride probe status is further set as questionable.)
$T_{th(n)} \le t_n$	$T_n = T_{n-1} - (t_n - t_{n-1})$ (Chloride probe status is further set as questionable.)	$T_n = T_{add}$	$T_n = T_{add}$

If corrosion rate sensor is not normal, $T_n = T_{th(n)} - t_n + T_{add}$.

2) If two chloride probes and the corrosion rate sensor are normal, use the following table to calculate service life.

	$CR_n < 0.1$	$0.1 < CR_n < 1$	$CR_n > 1$
$T_{th(n)} > t_n$	$T_n = T_{th(n)} - t_n + T_{add}$	$T_n = T_{th(n)} - t_n + T_{add}$	$T_n = T_{add}$ (Chloride probe status is further set as questionable.)
$T_{th(n)} \le t_n$	$T_n = T_{n-1} - (t_n - t_{n-1})$ (Chloride probe status is questionable.)	$T_n = T_{add}$	$T_n = T_{add}$

If corrosion rate sensor is not normal, $T_n = T_{th(n)} - t_n + T_{add}$.

3) If only one chloride probe and the corrosion rate sensor are normal, use the following table to calculate service life.

	$CR_n < 0.1$	$0.1 < CR_n < 1$	$CR_n > 1$
$T_{th(n)} > t_n$	$T_n = T_{n-1} - (t_n - t_{n-1})$	$T_n = T_{n-1} - (t_n - t_{n-1})$	$T_n = T_{add}$ (Chloride probe status is further set as questionable.)
$T_{th(n)} \le t_n$	$T_n = T_{n-1} - (t_n - t_{n-1})$ (Chloride probe status is questionable.)	$T_n = T_{add}$	$T_n = T_{add}$

4) If no chloride probe is normal and the corrosion rate sensor is normal, use the following table to calculate service life.

$CR_n < 0.1$	$0.1 < CR_n < 1$	$CR_n > 1$
$T_n = T_{n-1} - (t_n - t_{n-1})$	$T_n = T_{n-1} - (t_n - t_{n-1})$	$T_n = T_{add}$

If the corrosion rate sensor is not normal, then $T_n = T_{n-1} - (t_n - t_{n-1})$

Note that the current QC algorithms assume one-directional diffusion of chloride into concrete and the chloride probe 3 at the depth of the rebar of interest. As such, the algorithms will need to be modified for the case of ODOT concrete girder, which features two-directional diffusion of chloride into concrete and the embedment of chloride probe 2 at the depth of the rebar. The current QC algorithms, however, have laid the groundwork for further improvements of the software.

2.5.3. Software Interface

A software package is developed based on the algorithms and data QC schemes provided above. The main interface is shown in Figure 22, which includes (remaining) service life prediction, sensor status, and display of historical data. The detailed code of the software is available from the WTI CSIL upon request.
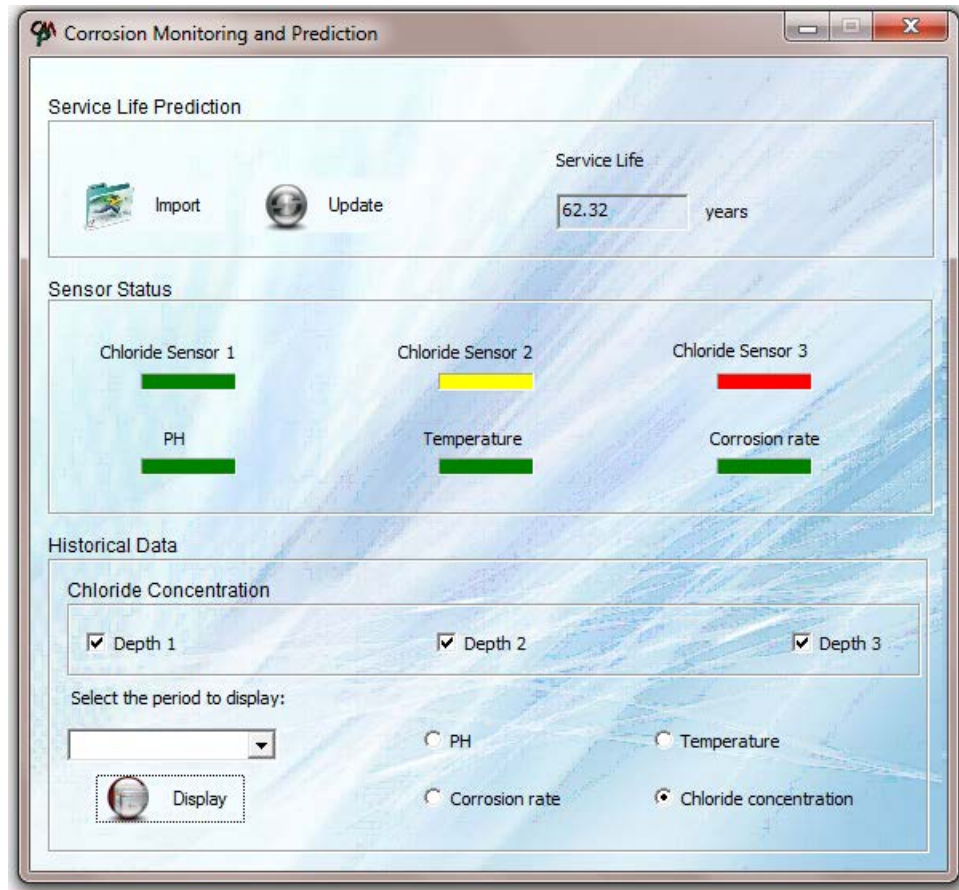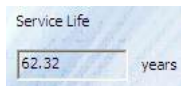

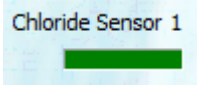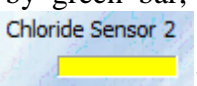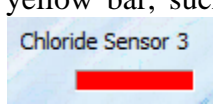**Figure 21.** Main user interface of the corrosion sensing system

Under Service Life Prediction, the "Import" button ( ) allows users to open, select, and import new data set that will be incorporated into the analysis. When the mouse cursor is over the "Import" button, the software shows the hint: " Select the new dataset for analysis ". A window, as shown in Figure 23, will be open when click on the "Import" button. As the final format of the raw data file is not yet provided by SwRI, this function is currently disabled.
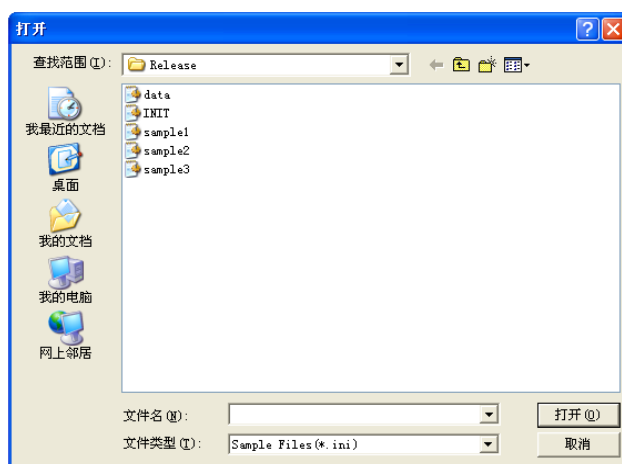
Figure 22. User interface to import sensor data

The "Update" button ( ) is to calculate and update the service life of the associated infrastructure and the result is shown in the under the text "Service Life" ( ).When the mouse cursor is within the "Update" button area, the software shows the hint: " Calculate service life of the infrastructure ".

Under the sensor status section, the interface displays the status of the three chloride probes, PH sensor, temperature sensor, and corrosion rate sensor. Sensor status include "normal" (indicated by green bar, such as), "questionable" (indicated by yellow bar, such as), and "malfunctioning" (indicated by red bar, such as).

The software also provides access to historical data for all of the sensors. By selecting the sensor (Chloride Concentration, pH, temperature, etc) and time period (30 days—30D, 90D, 180D, 1Y, 3Y, 5Y, ALL), clicking on the "Display" ( ) button, a pop-up window shows the desired historical data. Figure 24 shows an example of displaying

historical chloride probe data. Note that the legend and units in Figure 24 will be revised later on, depending on the user requirements.
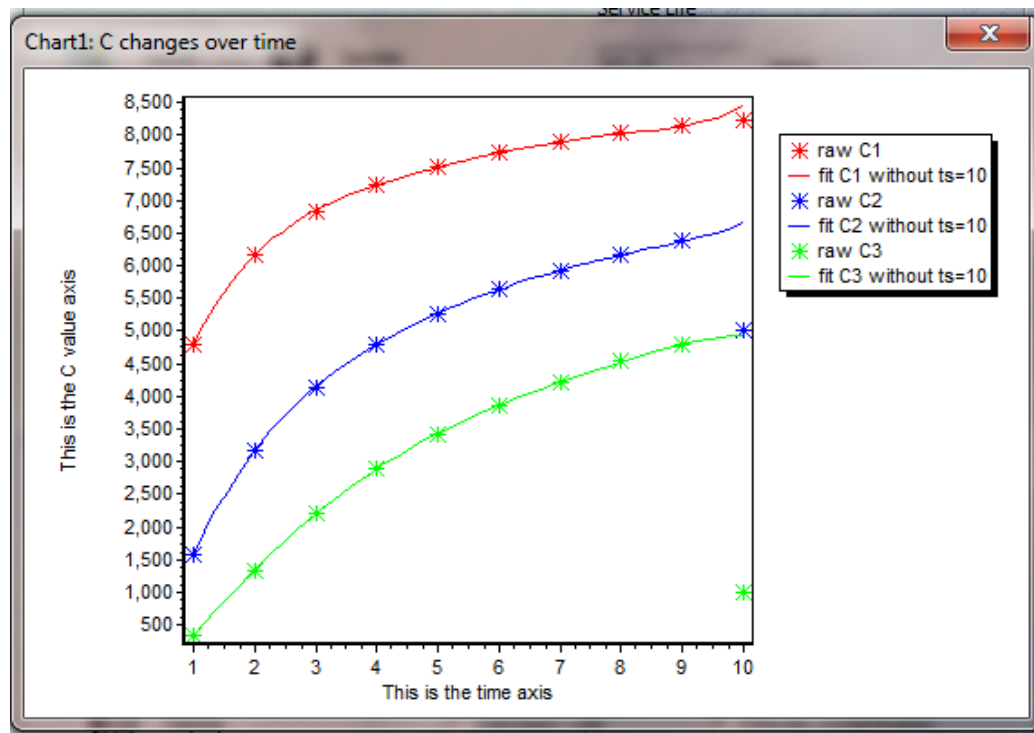
Figure 23. User interface to display historical sensor data

CHAPTER 3 - INTERPRETATION, APPRAISAL, AND APPLICATIONS

3.1 Guidelines for Sensor Field Implementation

This section describes in detail the components included in the delivered system and the steps necessary to successfully install the system in field location. It will take operators from the steps of identifying the parts that are sent to the field and how to install everything from the wire connection between parts to successfully acquire data from the system.

3.1.1. Parts for the Corrosion Sensing System

The summary of the components in the corrosion monitoring system is listed in Table 6.

Table 6. Components included in the delivered corrosion monitoring system

No.	Item & Description
1	1 x Sensor Set Includes: 1) three chloride probes and three graphite reference probes; 2) two 9-pin MAS probes and 3) one thermometer probe. The picture of the sensor is shown in Figure 24
2	1 x Aginova Sensor Platform (with supportive plate) Includes: 1) One Aginova MAS board (sensor ID: 8141) and 2) Two Aginova Sentinel Chloride board (Sensor ID: 9216 and 9226). The picture of the platform is shown in Figure 25
3	1 x NETGEAR Wireless-G Router (WGR6 14 v9) The picture of the router is shown in Figure 26
4	1 x Laptop (Dell Latitude D531 Laptop) and 1 x Aginova Software (Gold Version) The picture of the laptop with Aginova software is shown in Figure 27
5	1 x APC Back – UPS The picture of the UPS is shown in Figure 28
6	1 x Wire Cable connecting Router to Laptop (see Figure 30)
7	1 x Wire Cable connecting Router to UPS (see Figure 30)
8	4 x Battery for MAS board The picture of the battery is shown in Figure 29
9	8 x Battery for Chloride Board The picture of the battery is shown in Figure 29
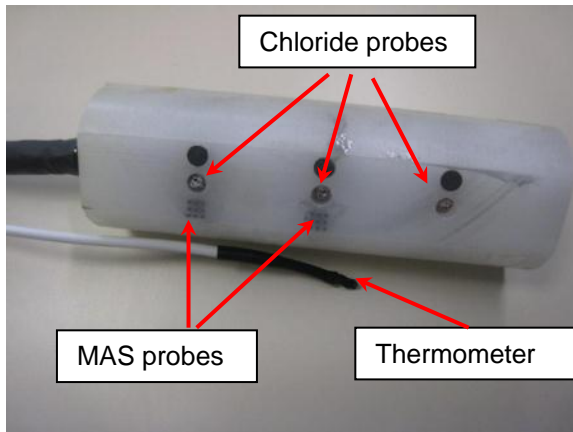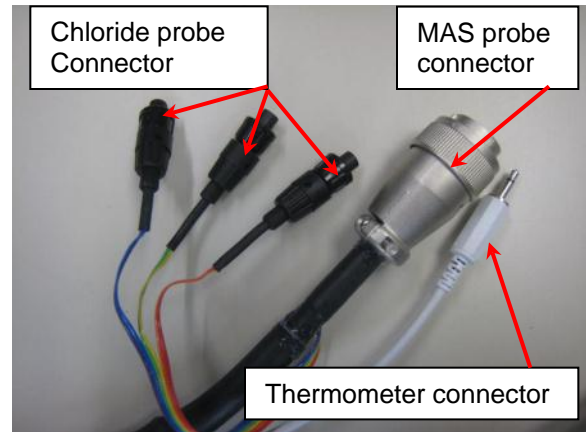
Figure 24. Corrosion monitoring sensor. (a) sensor body and (b) connectors
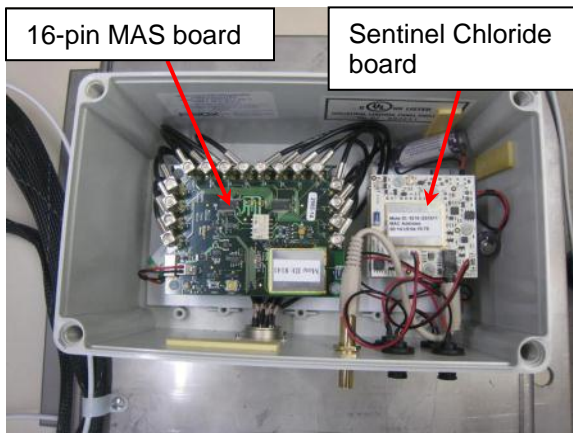
Figure 25. Aginova Sensor Platform (with supportive plate) (a) top view and (b) front view

Figure 26. NETGEAR Wireless-G Router (WGR6 14 v9)
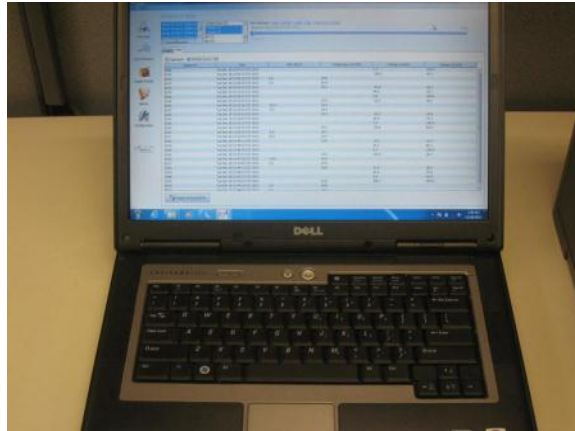
Figure 27. Laptop (Dell Latitude D531 Laptop) with Aginova Desktop Software (Gold Version) embedded

Figure 28. Power supplier (APC Back – UPS) for the Router

| (a) | (b) |

Figure 29. Backup batteries (a) for MAS board and (b) for chloride board

3.1.2. Step-by-step Field Implementation Procedure

The detailed procedure for field implementation is described as follows.

1) Identify the components in the system and check the sensor platform

Once the system was delivered, the DOT engineer should unwrap the box and identify the components in the delivery. Although well packed before shipping the platform, the components within the platform box may move and dislocate from the appropriate location due to the vibration in the shipping process. After delivery, operator should open the platform box to check if the components and wire connection are well fixed in the appropriate location.

After delivery, the integrity of sensor set should be carefully checked. If there is integrity issue regarding the sensor body or the connectors, please contact engineer at SwRI. If sensor probe surface was contaminated, please slightly polish with fine sand paper and then clean with DI water.

2) Install the batteries into the board

To avoid the board batteries in the platform move and break the board during the shipping process, they were disassembled before shipping and will be shipped separately. Therefore, the batteries will be re-set before monitoring. The re-set process is described as below in detail and a document with a video demonstration of installation process will be included within the deliverables. Note that a total of three batteries and one battery for each individual board will be re-set into the sensor platform.

The large "C" type batteries in a separated plastic bag will be used for the 16-pin MAS board and the "AA" style batteries in another plastic bag will be used for the chloride boards. All batteries are well wired with an appropriate connector. In the installation, first, the four screws on the cover of the platform should be removed with screw driver. Prior to install the battery, please double check the switch in each board is on the "off". Next, use the screwdriver to remove the four screws which holds down the upper chloride board. Then remove the upper chloride board from the box carefully. Subsequently, remove the four standoffs on the lower chloride board with a screwdriver and take out the lower chloride board from the box.

A connector for the battery can be found at the bottom side of the lower chloride board. Attach one "AA" type battery to the connector. Put the board back in and fix the battery with a tape. Screw the four standoffs back to the lower board. Then attach another "AA" type battery to the upper board through the connector at the back side of the board and then place the board back in. Mount the four screws on with the screwdriver. Double check if the two chloride boards are fixed in the appropriate location.

A connector on the front side of the MAS board can be found. Connect the "C" type battery to the MAS board through the connector. Turn all switches of three boards from "off" to "on" and the green LED lights on the three boards should be "on" momentarily. Screwdriver may be needed to help turn the switches on the chloride bards "on". If the LED light on a specific board does not "on", please check

the battery connection and re-connect it if necessary. In the end, put the cover back on and tight the screw down.

3) Wire connect components within the system

This work includes two parts. One is connecting the sensor set with the platform and the other is wire connecting the router, the laptop and the power supplier, UPS. Except the word and photograph description as below, a video record demonstrates the connection process for each part will be included in the deliverables. Watch the video before wire connecting the components will help setup the system correctly.

First, check the compatibility of the sensor connectors with the connectors embedded in the platform. Note that within the connector, only three chloride probe connectors are weather proof but the connectors for MAS and thermometer probes are not weather proof. It would be helpful to prevent the attack of humidity during severe weather environment if tape or silicon coat applied on the connection after plugging in.

Plug the 16-pin round MAS sensor connector (military connector) through lining the notch with the notch of the connector in the platform box. Push the MAS connector fully in and tight the connector until stop. The connection between the chloride probe connectors and connectors on the platform box can be identified with the color code of the connector wire and written on the platform box. Put the notch of the sensor wire connector in a line with the notch of the connector in the box. Then push it in, spin until click. Conduct these two connections one by one. The pin connector for the temperature sensor will be connected by pushing straight in the connector on the box. The wire with RED color transfer data achieved from the top chloride probe, which is close to the connection wire. The wire with GREEN and BLUE colors transfer data achieved from the middle and bottom chloride probe, respectively.

Figure 30 shows the wire connection of router, laptop and UPS. Note that the UPS should be fully charged (at least to be charged for four hours in office building and prefer to be charged overnight) before each field usage. Our test indicates that the UPS can continuously supply power to the router for more than 5 hours, which is more than enough for router to communicate with the platform and download two-year data collected and storage in the board. During working, the UPS gives "bi, bi, bi" noise in every couple minutes, which is because it is not wire connected to an AC power resource. This is normal and no action should be conducted to solve it. Also note that during the filed data acquisition process, the components, including laptop, router and UPS, should be placed less than 100 feet from the platform.

The networks cable wire connects the laptop and the No.1 connector of the router. The power wire will be plugged to the router and the battery side of the UPS. Turn on the laptop. No user name and password have been pre-set for this laptop. Double click the icon "Aginova" on the desktop and the software interface shown on the screen. Note that the laptop uses its own battery in field operation. The UPS only provide power to the router. The router will pick up all data collected and storage in the platform in a specific time interval.

(a)

(b)

Power wire connecting router and UPS

Data wire connecting router and laptop
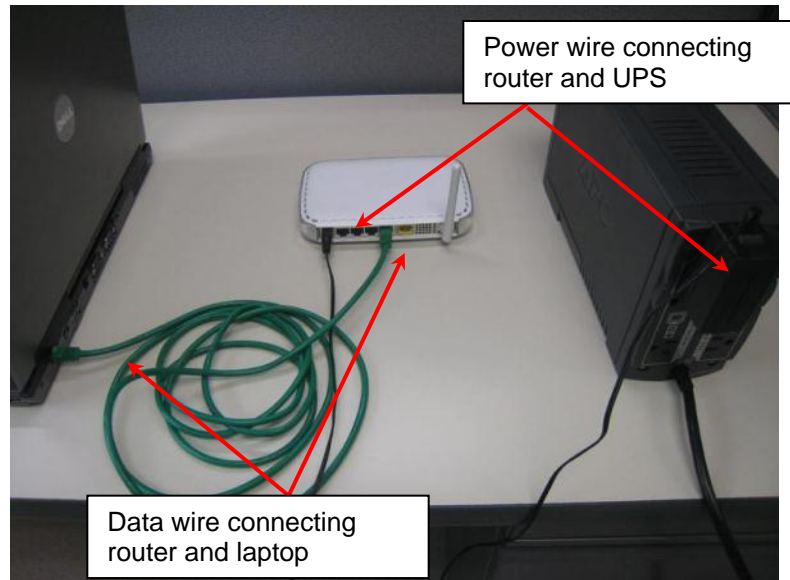
(c)

Figure 30. Wire connection for router, laptop and the UPS (a) router (back view), (b) UPS (back view) and (c)

4) Implement sensor body and platform

In the structure, select a location where represents the most severe chloride attack and rebar corrosion occurrence to embedded the sensor body. A cylindrical hole with 2 ½" diameter and 6″ depth will be drilled at the selected location. The hole should be 45° downward from a top surface of the structure. The sensor body will be fully embedded in the middle of the hole. The paste provided by MSU will be used to fill the space between sensor and the structure tightly. Note that when embedding the sensor body into the structure, the flat surface with probes should be faced upwards and to the concrete surface which exposure to most severe attack of chloride. Also note that no rebar touch the sensor directly.

The platform will be placed near the embedded sensor body. To avoid the stress on the connection wires, the distance between the platform and the sensor should be less than 5 feet. Further, the platform is preferred to be placed in a shielded space. The platform will be fixed on a flat surface of the structure through mounting the supportive plate with four 5/8" bolts. After mounting the plate, open the platform cover and turn the power switch button on. Then tightly screw down the cover to seal the platform.

5) Test the workability of the system

To test the workability of the whole system, the acquisition frequency for data from all probes was pre-set as three minutes in the software when the system is delivered. Therefore, after the batteries installed and the power switch button of boards turned on, the platform starts to pick up data from the three boards several minutes later. In each three minutes interval, there are a total of 16 "click" noises from the platform, which indicates that the MAS board is picking up data from MAS

probe. Similarly, the chloride boards pick up data from chloride probes and thermometer probe in every three minutes but with no noise heard.

Then conduct the following procedure as a sequence of wiring connection the whole data acquisition components (router, UPS and the laptop), turning on the laptop and then double clicking the "Aginova" program. In the software interface, click the "List of Sensors" icon on the left side of software approximately 10 minutes later. All available sensors, including MAS sensor, three chloride probes and one thermometer, will be listed. If a sensor appears in "Green" which means that the target sensor probe and it is in communication with the software. If a specific sensor appears "black", representing that the sensor is not response to the communication inquiry from the router. Then following check process should be performed in sequence. 1) if the probe and the platform connected well through wire; 2) if the power button on the board is "on"; and 3) if the UPS and battery of the laptop works. If there is still no response in half an hour, please shut down the laptop and un-plug cables, connections. Then repeat the process from the beginning to check if there is still no response from that specific probe. If is still doesn't work, please contact to SwRI personnel for helping.

It is to be noted that the data of MAS probe shown in the software are the raw data of each individual electrodes. The data column 0-7 represent raw data from electrodes 0 to 7 and the data column 8-16 represent raw data from electrodes 8 to16. The two groups of data represent the results of top and middle of MAS probe, respectively. When DOT engineer download the two groups of data and transfer to spreadsheet format and then send to engineer at SwRI, the data will be analyzed; the results of rebar corrosion rate and mass loss will be achieved.

If the test passed, please adjust the data acquisition frequency for all sensor probes to 6 hours, which will guarantee to achieve enough data for subsequent analysis and simultaneously, save the battery to sustain the board for a longer service life. The process to adjust the sampling period is described as below. When all available sensors are "green" you can change the acquisition rate by checking the box next to one or up to all sensors then click the "configure selected sensors" button at bottom of screen. A new window will open up with various options to change. Input a new time interval in the "sampling period" in seconds to change acquisition rate.

Note that the unit of input time interval is second. If the sampling period is 6 hours, the input data should be "21600". When ready to change click the "schedule reconfiguration" button at the bottom to initiate reconfiguration. It will take several minutes for the reconfiguration to be performed on the sensor(s). To verify that the sensor(s) has been reconfigured, go to "List of Sensors" and click the sensor you wish to check. The details regarding the inquired sensor will be highlighted and displayed on the screen. "Sampling" is the sampling rate for that sensor.

Once system passed the testing, the data acquisition components, including laptop, router and UPS will be dissembled and shut down for next field data collection. It is expected that the DOT engineer has a site visiting and download the data storage in the board in every 3 months.

6) Download data periodically

In every periodical onsite visiting, the DOT engineer will bring the router, USP and laptop to the field to check the workability of the system and download data storage in the board. As described in step 3), wire connect the router, USP and laptop in less than 100 feet from the platform and turn the laptop and open the software. First, the "Overview" interface shown on the screen. Click the "Graph and Data" icon on the left of screen to switch to the data view. Click the "Data" Tab to see the spreadsheet style view of the data. Select all available sensors from the sensor list box. Select all available data types from the data type list box. Next select the time period you wish to see from the option tab on the top of the interface. The slide bar can be used to further refine the time period of data you wish to view. Allow the data to update and then click the "Export to Excel" Button at the bottom of the software. Input a name to the file a name and click "save". The data file can be sent to SwRI and MSU for analysis and discussion.

3.2. The Sensor Embedment Method

At the WTI CSIL, various mortar mixes were designed and tested for their potential use for embedding the corrosion sensing system. Experimental testing focused on the workability and initial setting time of fresh mortar mixes, the 28-day compressive strength of hardened mortar mixes as well as their modulus of elasticity, bond strength on old concrete, chloride diffusion coefficient, and coefficient of thermal expansion. A comprehensive examination of the experimental data led to the selection of two highly flowable, self-consolidating mortar mixes for embedding the corrosion sensing system.

Note that the sensor probes will be set into the outer surface of the thin-walled elastomeric tube with the electrical connection wires extended from the inside of the tube. The tube will be then filled with high performance epoxy. The sensor and tube assembly will be placed in a hole drilled at a downward angle near the bottom of a concrete girder. The drilled hole can simulate the case where a concrete core is extracted from field RC structure for chloride profiling. The extracted core will be tested to assess the chloride concentration profile of the existing concrete. Extreme caution will be exercised to avoid the risk of getting broken cores or leaving broken pieces in the hole. The central MAS probe (unit 2) will be within 1 inch of the steel reinforcement, while the three chloride probes will be used to monitor the evolution of chloride concentration depth profile over time.

The sensor embedment method is illustrated in Figure 31. The primary goal is to minimize the potential disturbance of such embedment on the local environment to be monitored for the risk of rebar corrosion in concrete. A total of three materials will be used sequentially for embedding the corrosion sensing system and it may take three field trips to complete. These include: mortar mix 1B, mortar mix 1A and Marine Epoxy. Both mortar mixes are highly flowable in their fresh state once mixed correctly; their hardened-state compatibility with existing old concrete has been validated in the WTI CSIL.
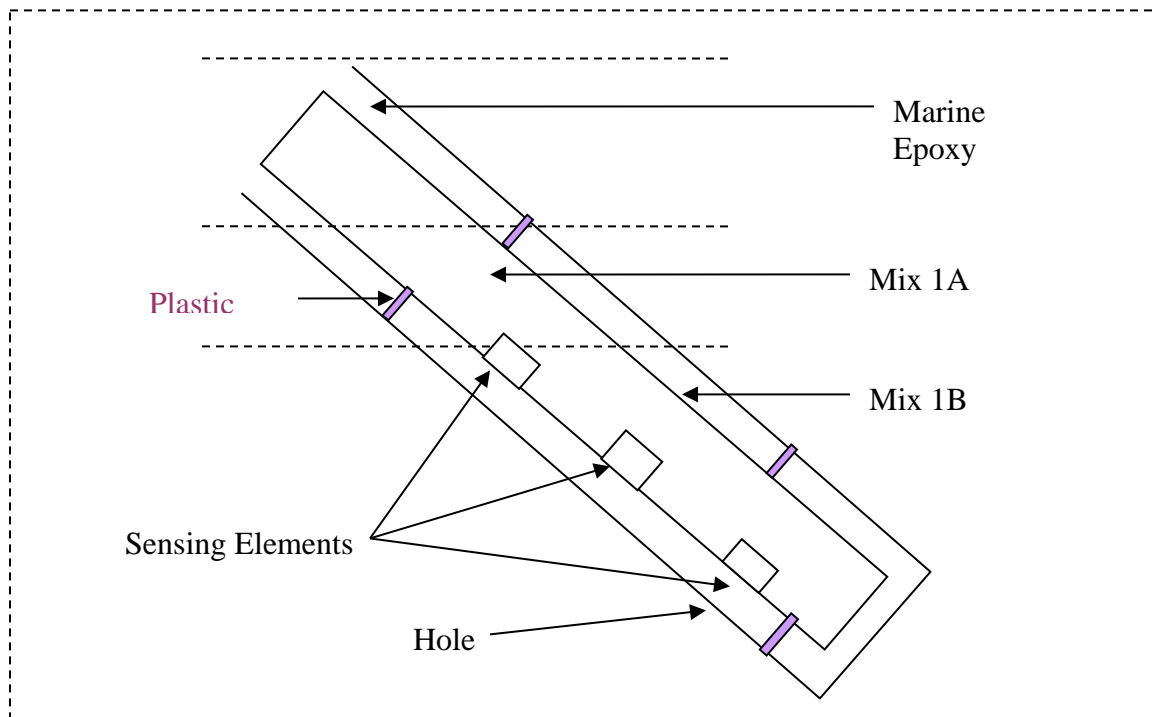
Figure 31. Schematic illustration of the sensor embedment method

Step 0. Clean the drilled hole with paper towel and compressed air to ensure that the surfaces are free of debris, free water or other contaminants.

Step 1. Drill four small holes (e.g., 1/8" in diameter and depth) on the white polypropylene cylinder body of the corrosion sensing system. Avoid areas with exposed sensing elements. Drill these four holes at various depths and sides of the cylinder. Do not drill too deep so that the interior of the sensor wires are free from potential damage by the drilling.

Step 2. In each of these drilled small holes push in a plastic cylinder (1/8" in diameter and 5/8" in depth). Note that this leaves separation between the sensing elements and the inside (surface) of the hole" to be 0.5" and the mortars will be able to flow thru such "crevices".

Step 3. Push the corrosion sensing system (now with four small plastic plugs protruding out) all the way into the hole where the concrete girder was cored (the hole is 2.5" in diameter and 5" deep and 45 degrees downward facing the ground). Make sure that the sensor side with all the sensing elements is facing downward.

Step 4. Now that the corrosion sensing system is fixed inside the hole in the concrete girder, sealing of the hole can begin.

Step 5. First, mix the solid and liquid components of Mix 1B together (consisting of water, cement, fine sand, carbon microfiber and nanoclay) and add a certain amount of Calcium Chloride (CaCl2.2H_2O) into it. The appropriate amount is based on the measured chloride concentration profile of the concrete core taken from the girder. Agitate for 10 minutes to obtain best possible uniform distribution of various

61

components. Note that only about 206 mL of this fresh mortar mix 1B (roughly estimated to be 495 g) will be poured into the concrete hole, with the goal of just embedding all the sensing elements yet leaving room in the hole for the other embedding materials. This adds a layer of highly permeable mortar to embed the sensing elements, which allows quick equilibrium of chloride content with the adjacent concrete. The volume of 206 mL (highly permeable mortar) is able to fill in the hole for about 3.2" if the hole is not 45 degrees but rather straight.

Step 6. Leave this 1st mortar mix (1B) to flow flat and set in the field for at least 6 hours before proceeding to the 2nd mortar mix (1A).

Step 7. Second, mix the solid and liquid components of Mix 1A together (consisting of water, cement, fine sand, carbon microfiber, nanoclay, SBR, TEA, and calcium nitrite). Agitate for 10 minutes to best possible uniform distribution of various components. Note that only about 129 mL of this fresh mortar mix 1A (roughly estimated to be 309 g) will be poured into the concrete hole (on top of the set 1st mortar mix), with the goal of adding a layer of highly impermeable mortar that would minimize the ingress of external chlorides, moisture and other contaminants into the concrete. The volume of 129 mL (highly impermeable mortar) is able to fill in the hole for about 2" if the hole is not 45 degrees but rather straight.

Step 8. Leave this 2nd mortar mix (1A) to flow flat and set in the field for at least 12 hours before proceeding to the 3rd materials (Marine Epoxy).

Step 9. Third, pour about 58 mL Marine epoxy into the hole (on top of the set 2nd mortar mix). This is for further minimize the ingress of external chlorides and moisture into the concrete.

Even before the epoxy sets (typically after 24 hours), the embedment is complete and the embedded sensing system is ready for tests.

CHAPTER 4 – CONCLUSIONS AND SUGGESTED RESEARCH

4.1. Conclusions

This study has developed and evaluated in the laboratory a multi-parameter corrosion monitoring system for existing reinforced concrete structures in chloride-laden service environments. The study improved and validated the SwRI corrosion sensor prototype for use in the concrete corrosion monitoring system; developed algorithms for quality control and interpretation of the sensor data; made viable recommendations to implement the corrosion monitoring system for existing DOT inventories of RC bridges; and delivered a deployable prototype corrosion sensing system for DOTs to continue field evaluations. The performance and reliability of the SwRI corrosion sensor were confirmed by the benchmark test in simulated concrete pore solutions. However, once active corrosion is initiated and a great amount of chloride is present, the multi-electrode array sensor (MAS) probe may no longer serve as a good tool to predict the corrosion rate of rebar unless more research is conducted to establish such prediction or correlation. The performance and reliability of the SwRI corrosion sensor were also confirmed by embedding it in a paste specimen, while some issues with firmware and possibly graphite reference probe were identified. While more research is needed, the paste specimen test also imply that the MAS probes, Cl probes and pH probes all have great potential to work properly under a reasonably low electric field.

At the WTI CSIL, the custom-made chloride probes along with the SwRI sensor, a conventional Ag/AgCl probe (as control), and three rust-free, bare steel #4 rebars went through a cyclic immersion in the simulated concrete pore solutions. For the 9-pin MAS, the following three parameters showed strong correlation with the chloride concentration of the simulated pore solutions: (1) *maximum of maximum ΔE*, (2) *maximum of average ΔE*, and (3) *average of average ΔE / average of maximum ΔE*. For the 6-pin MAS, the following three parameters showed strong correlation with the chloride concentration of the simulated pore solutions: (1) *average of maximum ΔE*, (2) *average of average ΔE*, and (3) *average of average ΔE / maximum of maximum ΔE*. The 3rd parameter may hold the promise of using 6-pin MAS as a very good tool to predict the rebar corrosion rate even in the case of active corrosion and high chloride concentration, which warrant additional research. Only one of the three SwRI Ag/AgCl probes was found to be reliable chloride probes after the eight cycles of weathering. This highlight the need for further improving the approach to fabricate the Ag/AgCl probes to serve as chloride probes in concrete. Meanwhile, three WTI custom-made chloride probes (with the appropriate treatment by proprietary coating) showed great promise in this regard. Only one of the three SwRI graphite probes remained relatively stable over the eight cycles of weathering, with its potential showing a standard deviation of 11 mV and a COV of -6%. Interestingly, a few of the WTI custom-made Ag/AgCl probes showed good potential to serve as reliable reference electrodes in concrete. The vast majority of the sensing probes featured a response time of less than 60 seconds.

4.2. Implementation Recommendations

To facilitate the technology transition into practice and to realize the substantial benefits inherent in this technology, the researchers will work closely with ODOT and other DOT end

users and other stakeholders to produce a technology that meet user needs, are cost-effective, and can be readily implemented.

A successfully deployed system in the field RC structure would provide owners and maintainers of RC structures, engineers, architects, contractors, and other stakeholders with an improved understanding of the evolution of rebar corrosion, and environmental factors affecting concrete degradation. This will lead to best practices of corrosion management. A deployed system on a bridge will have a network of sensors operating continuously, which will provide far more information at less cost than the current labor-intensive method of collecting chloride depth profiles. The analysis methods applied to the time-series data will be able to extract more accurate condition information relative to the limited periodic data collected through the coastal surveys. The monitoring system will provide higher quality corrosion condition information at less cost. This technology will detect corrosion initiation and propagation in RC structures at the earliest possible time, enabling condition-based maintenance strategies. Further, it will provide increased reliability and remote-sensing capability for condition assessment and service life prognosis of RC structures, enabling lifecycle performance assessment of corrosion-affected RC structures.

At this stage, there are several technical challenges identified for the proposed monitoring system. First, long-term durability and survivability of sensors in the heterogeneous, highly alkaline concrete matrix presents a significant challenge, particularly for the chloride probes and reference probes. The RC structures in the field environment are exposed to wet–dry and temperature cycling, which adds to the challenge. Appropriate selection, design and manufacturing of the sensor probes will be needed to mitigate such concerns. Furthermore, the software program will be used to filter the noises in the sensor measurements from the signals. Secondly, the long-term reliability of the overall monitoring system in the field environment is a concern. The use of low power wireless data acquisition hardware will help address this concern. Most power consumption occurs during data transmission. We propose to acquire data every 6 hours but upload data only once per month, significantly increasing battery life. Further, the electronics housing will be external to the concrete with only the probe embedded into the structure, facilitating battery replacement or the implementation of solar power.

4.3. Suggested Research

In light of findings from this study, the following research needs are identified.

- Additional optional phases of this project should focus on improving the system reliability, usability and cost-effectiveness.

- Additional research should examine the feasibility to use a certain parameter from the 6-pin MAS probes, such as *average of average ΔE / maximum of maximum ΔE* or certain index calculated from the MAS probe readings (e.g., localized index using the software of *electrochemical noise analysis*) to reliably predict the rebar corrosion rate even in the case of active corrosion and high chloride concentration.

- Research is warranted to evaluate the combined use of the developed corrosion sensing system with ICCP to automatically adjust the protective current in a way that maximizes

anode life and optimizes corrosion control. This may also entail the strategic placement of the sensing probes.

REFERENCES

[1] Tuutti, K. Service life of structures with regard to corrosion of embedded steel. Performance of concrete in marine environment, ACI SP-65. Detroit, Michigan: American Concrete Institute; 1980. p. 223-36.

[2] Weyers, RE. Service life model for concrete structures in chloride laden environments. ACI Mater J 1998, 95 (4), pp.445–53.

[3] Maaddawy, T.E., and K. Soudki. A Model for prediction of time from corrosion initiation to corrosion cracking. Cement & Concrete Composites, 29, 2007, pp.168-175.